



# 3D reflection seismic imaging of natural gas/fluid escape features in the deep-water Orange Basin of South Africa

N. G. Maduna<sup>1</sup> · M. S. D. Manzi<sup>1</sup> · J. E. Bourdeau<sup>2,3</sup> · Z. Jinnah<sup>1</sup>

Received: 17 December 2022 / Accepted: 2 May 2023 / Published online: 25 May 2023  
© The Author(s) 2023

## Abstract

Many features indicative of natural gas and oil leakage are delineated in the deep-water Orange Basin offshore South Africa using 3D reflection seismic data. These features are influenced by the translational and compressional domains of an underlying Upper Cretaceous deep-water fold-and-thrust belt (DWFTB) system detaching Turonian shales. The origin of hydrocarbons is postulated to be from both: (a) thermogenic sources stemming from the speculative Turonian and proven Aptian source rocks at depth; and (b) biogenic sources from organic-rich sediments in the Cenozoic attributed to the Benguela Current upwelling system. The late Campanian surface has a dense population of > 950 pockmarks classified into three groups based on their variable shapes and diameter: giant (> 1500 m), crater (~ 700–900 m) and simple (< 500 m) pockmarks. A total of 85 simple pockmarks are observed on the present-day seafloor in the same area as those imaged on the late Campanian surface found together with mass wasting. A major slump scar in the north surrounds a ~ 4200 m long, tectonically controlled mud volcano. The vent of the elongated mud volcano is near-vertical and situated along the axis of a large anticline marking the intersection of the translational and compressional domains. Along the same fold further south, the greatest accumulation of hydrocarbons is indicated by a positive high amplitude anomaly (PHAA) within a late Campanian anticline. Vast economical hydrocarbon reservoirs have yet to be exploited from the deep-water Orange Basin, as evidenced by the widespread occurrence of natural gas/fluid escape features imaged in this study.

**Keywords** Deep-water Orange Basin · 3D reflection seismic data · Gas/fluid escape feature · Pockmarks · Mud volcano · PHAA anticline

## Introduction

The southwest African passive margin has received much interest pertaining to the economical hydrocarbon systems found within the Orange and more southern Outeniqua basins (e.g., van der Spuy and Sayidini 2022). Deep-sea technological advances made by the petroleum industry since the 1970s have allowed the more distal regions of sedimentary basins to be explored. This has promoted interest in the study of complex geological structures known to either host or are indicative of gas/fluid migration. The expression of fluid and gas migration through the sedimentary column is shown by a variety of features such as: gravity collapse structures, mounds, mud volcanoes, surface and buried pockmarks, diapirs, cold seeps and polygonal faulting (Cartwright et al. 2007; Hartwig et al. 2012; Ho et al. 2012). These features are often associated with seismic anomalies such as positive high amplitude anomalies (PHAAs), bottom simulating

✉ N. G. Maduna  
nombuso.maduna@gmail.com

M. S. D. Manzi  
musa.manzi@wits.ac.za

J. E. Bourdeau  
bourdeau.julie.e@gmail.com

Z. Jinnah  
zubair.jinnah@wits.ac.za

<sup>1</sup> School of Geosciences, University of the Witwatersrand, Johannesburg, South Africa

<sup>2</sup> Geological Survey of Canada, 601 Booth Street, Ottawa, ON K1A 0E8, Canada

<sup>3</sup> Wits Mining Institute, University of the Witwatersrand, Johannesburg, South Africa

reflectors (BSRs), and pipe and chimney venting structures (Løseth et al. 2011; Gay et al. 2003; Cartwright et al. 2007; Hustoft et al. 2010; Ho et al. 2012). Natural gas/fluid escape features identified offshore South Africa and Namibia in the shallow Orange Basin include seafloor and buried pockmarks (Hartwig et al. 2012), seismic chimneys (Ben-Avraham et al. 2002; Paton et al. 2007; Kuhlmann et al. 2010; Boyd et al. 2011), mud diapers and volcanoes (Ben-Avraham et al. 2002; Viola et al. 2005), reflecting the basin's underlying hydrocarbon system. Economical hydrocarbon reserves are proven in the Orange Basin, both in the shallow and deep-water environments (Boyd et al. 2011; Isiaka et al. 2017; van der Spuy and Sayidini 2022). This is reflected by the Namibian Kudu and South African Ibbubhesi gas fields which are in production along the shelf, and the recent deep-water hydrocarbon finds in Namibia from the Graaf-1 appraisal and Venus-1X wildcat wells which are directly adjacent to this study (Fig. 1). Since the deep-water discoveries in Namibia are in proximity to this study, and the two regions are similar in geology, the potential for prolific hydrocarbon finds in the distal Orange Basin of South Africa is high.

The deep-water study area sits within a region of well-preserved Upper Cretaceous gravitational collapse structures, referred to as deep-water fold-and-thrust belts (DWFTBs) (Fig. 1; de Vera et al. 2010; Rowan et al. 2004; Nemcok et al. 2005; Paton et al. 2007). Key elements in the evolution of the Orange Basin have been constrained through various studies mostly using early 2D reflection seismic data, well logs, then much later 3D reflection seismic data (e.g., Light et al. 1993; Clemson et al. 1997; de Vera et al. 2010; Hartwig et al. 2012; Dalton et al. 2015, 2017; Collier et al. 2017; Baby et al. 2018; Mahlalela et al. 2021; Maduna et al. 2022). These studies describe events within the late stages of continental breakup, including the stratigraphy, structure and formation of gravitational collapse structures together with the hydrocarbon potential of the basin. The observations are however limited in South Africa since few studies have integrated the known hydrocarbon system with the natural fluid/gas features observed in relation to the underlying structure and stratigraphy of the passive margin, and even more so in the distal deep-water environments (e.g., Kuhlman et al. 2010; Mahlalela et al. 2021). Furthermore, in contrast to the Namibian extent, the deep-water Orange Basin remains underexplored in South Africa due to the sparsity of wells and limited 3D reflection seismic data coverage (Fig. 1; PASA 2017; van der Spuy and Sayidini 2022). The main aim of basin analysis is in understanding the basin's evolution which is centred around the tectonic setting under which the basin formed, its depositional environment, and the presence, accumulation, and extent of hydrocarbons. In this study we attempt to better constrain these elements

in the deep-water Orange Basin offshore South Africa. We use seismic attributes to resolve numerous natural gas/fluid escape features and describe their relationship to the underlying DWFTB system described in Maduna et al. (2022).

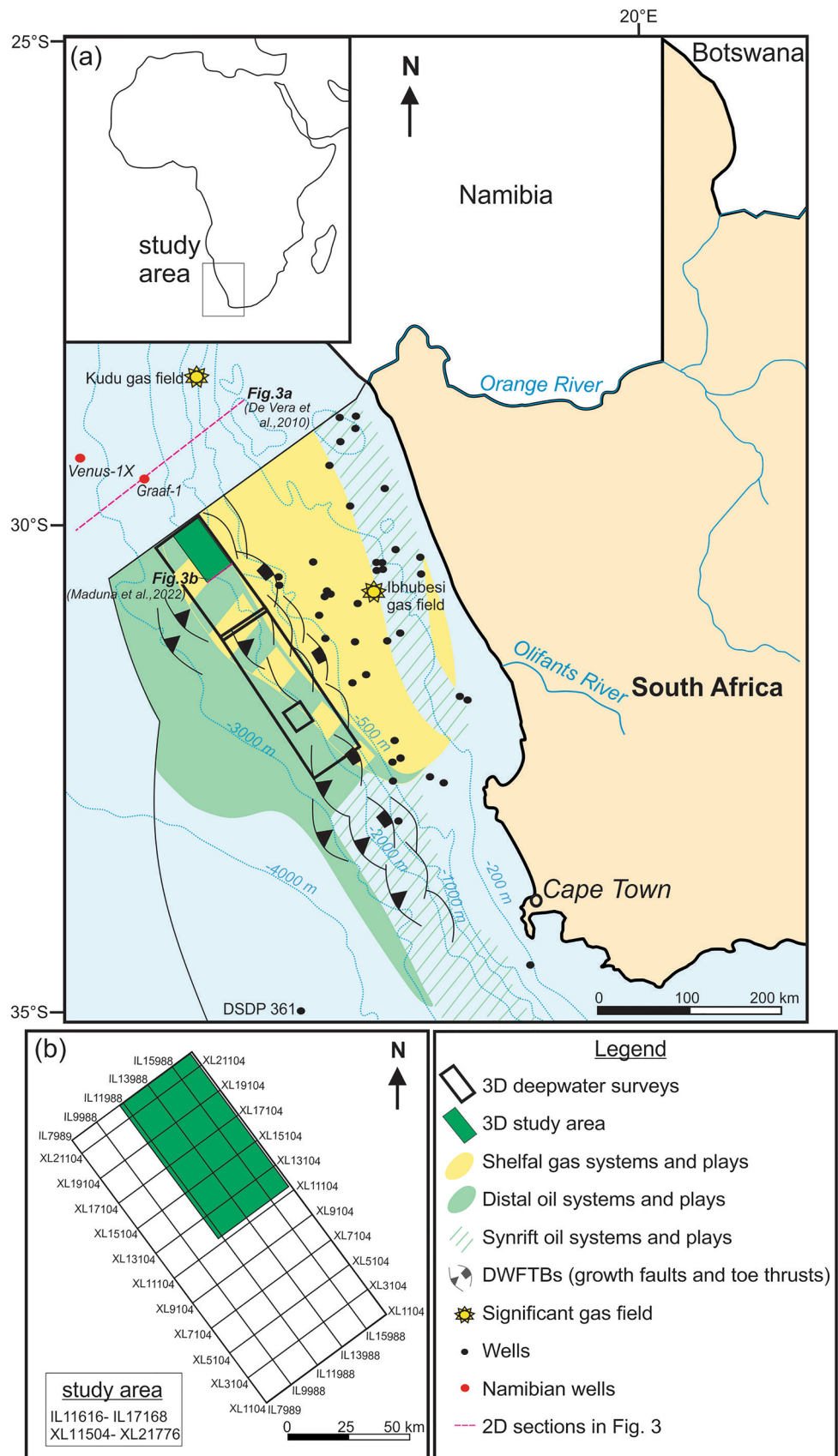
## Regional setting

The study area is located in the deep-water Orange Basin offshore SW Africa between 1000 and 2000 m water depths (Fig. 1). The basin covers an overall area of ~160 000 km<sup>2</sup> with the southern and central extents located offshore western South Africa and the northern extent located offshore Namibia. The Cretaceous to present-day infill of the Orange Basin is derived from the South African Plateau (SAP) (or hinterland) with sediment transported by the Orange and Olifants rivers and their proto-equivalents since the Lower Cretaceous (Maslanyj et al. 1992; De Vera et al. 2010). The sedimentary succession is comprised of syn-rift sequences related to the break-up of Gondwana during the Late Jurassic, followed by drift (post-rift) sequences with the opening of the South Atlantic (Fig. 2; Light et al. 1993). In the southern Orange Basin, the maximum depositional thickness is ~3 km, while in the north, the sedimentary succession reaches ~7 km (Kuhlmann et al. 2010). The structural and stratigraphic evolution of the SW African margin has been analysed mostly using seismic data and well logs, including the study of sediment accumulation rates, solid phase volumes and thermo-chronometric datasets (e.g., Light et al. 1993; de Vera et al. 2010; Hirsch et al. 2010; Baby et al. 2018, 2020; Maduna et al. 2022).

## Offshore structural framework

The pre-rift basement offshore SW Africa is comparable to the complex onshore Proterozoic to Early Paleozoic Pan African Gariep Belt (Clemson 1997; Frimmel et al. 2011; Mohammed et al. 2017). A 30 km wide, N–S orientated zone of pronounced flexure, known as the 'hinge line', has separated regions of uplift and subsidence since the Mesozoic in the pre-rift basement (Light et al. 1993; Clemson et al. 1997; Mohammed et al. 2017; Baby et al. 2018). The hinge line forms a critical boundary separating the margin's offshore and onshore morphologies (Light et al. 1993; Clemson et al. 1997; Aizawa et al. 2000) and its flexure reflects its progressive landward migration (Baby et al. 2018). The hinge line is offset by several NE–SW fracture zones (segment boundaries) which partitioned rifting during the break-up of Gondwana between the Middle to Late Jurassic (160 to 130 Ma) (Clemson et al. 1997). Seaward dipping reflectors (SDRs) observed in the upper

**Fig. 1** Map of the SW African margin showing **a** known and predicted hydrocarbon systems, wells, position of sections in Fig. 3, and DWFTBs in the South African Orange Basin; and **b** location of the present study area in green



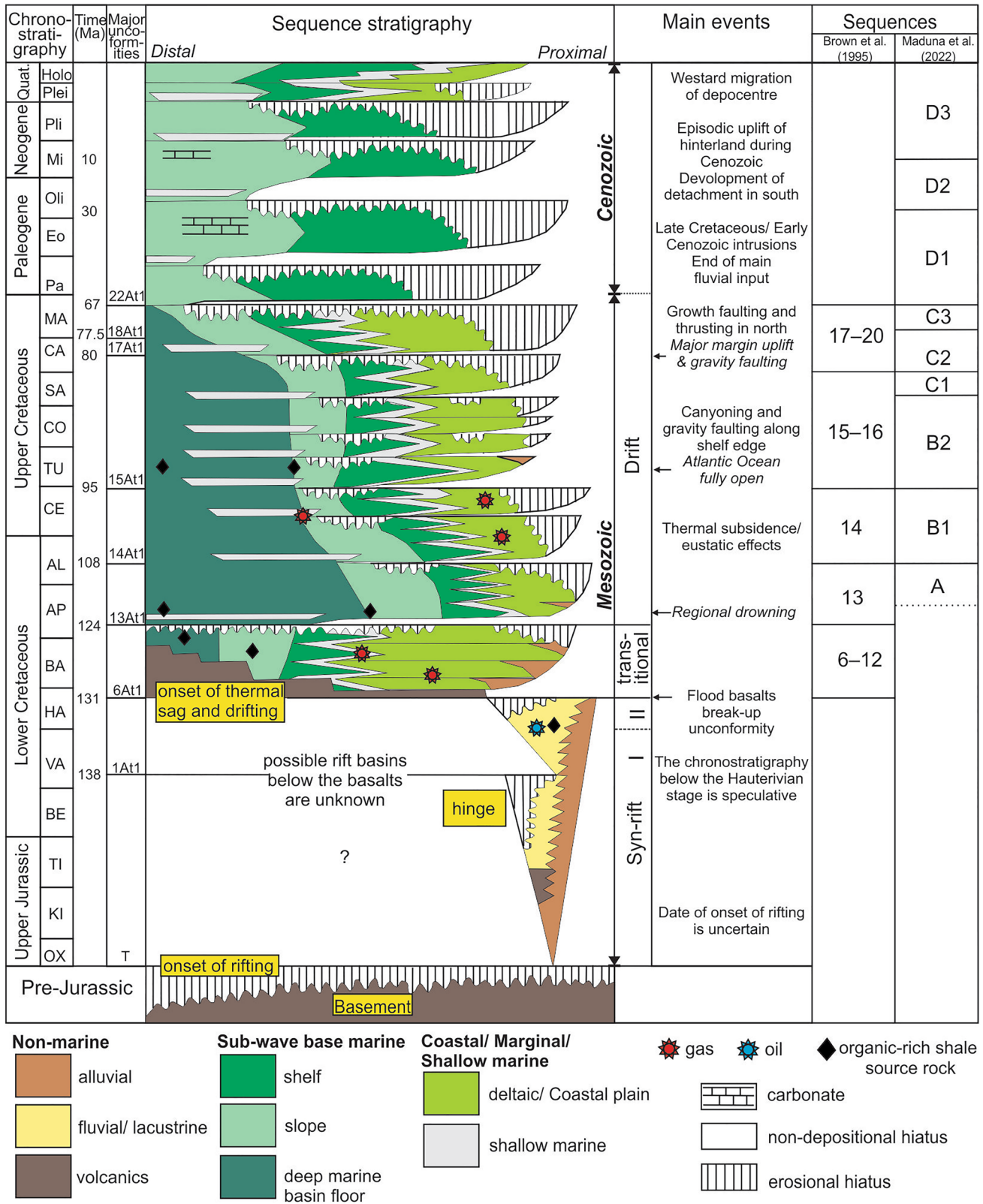


**Fig. 2** Chronostratigraphy and sequence stratigraphy of the Orange Basin throughout the evolution of the margin using the stratigraphic nomenclature developed by PetroSA (previously Soeker) (Brown et al. 1995; PASA 2017)



basement lithologies of the SW African margin reflect the volcanic evolution of the passive margin during rifting (Clemson et al. 1997; Menzies et al. 2002; Séranne and Anka 2005). The SDRs form a thick > 3 km package comparable in age to the Parana-Etendeka Large Igneous Province at ~ 135 Ma (Koopman et al. 2016; Baby et al. 2018).

The zipper-like south to north opening of the South Atlantic Ocean occurred through right-lateral strike-slip motion along the NE–SW fracture zones (Light et al. 1993). Viola et al. (2012) places the opening of the South Atlantic Ocean at ~ 134 Ma, following ENE–WSW extension and rifting. The spreading oceanic ridge marks the onset of drift; the second major phase of margin evolution following the break-up of Gondwana (Séranne and Anka 2005; Granado et al. 2009). The spreading centre propagated northwards over a 40 my rift-drift transition period (Viola et al. 2012), with drift subdividing the margin into well-defined shelf, slope and basal environmental settings (Light et al. 1993). The oldest evidence of mid-oceanic ridge activity and the transition to oceanic crust occurs at the M3 magnetic anomaly, between the Hauterivian and Barremian sequences at 127 Ma (Séranne and Anka 2005). The Orange, Lüderitz and Walvis basins formed in zones of greatest subsidence between the Rio Grande Fracture Zone to the north and Aghulhas-Falkland Fracture Zone to the south (Light et al. 1993; Clemson et al. 1997; Séranne and Anka 2005). The smaller Cape and Outeniqua basins also formed south of the Orange Basin. The predominant structural grain and trend of all structural lineaments is NW–SE to NNW–SSE, following the regional foliation of the SW African margin (Light et al. 1993; Wildman et al. 2015).

### Offshore stratigraphy

The presence of SDRs together with rotated and eroded extensional fault blocks in the syn-rift sequence are evidence of the tectonic control on sedimentation along the SW African margin during this time (Maslanyj et al. 1992; Light et al. 1993; Granado et al. 2009). The syn-rift sequence is comprised of isolated half-grabens infilled with interbedded Late Jurassic to Lower Cretaceous (late Hauterivian) siliciclastic and volcanoclastic sediments (Fig. 2; Jungslager 1999; Paton et al. 2008). The onset of drift began with the deposition of Lower Cretaceous to present-day post-rift clastic sediments above the Hauterivian break-up unconformity (Fig. 2; Light et al. 1993; Menzies et al. 2002; Granado et al. 2009; de Vera et al. 2010). Early drift sediments correspond to black shales and claystones, while late drift sediments are interbedded heterolithic shales and claystones (Dalton et al. 2017).

Sedimentation in the Upper Cretaceous was primarily driven by tectonics with climate and oceanic circulation playing little to no role as the difference in pole and equator temperatures were low (Maslanyj et al. 1992; Light et al. 1993; Granado et al. 2009; Uenzelmann-Neben et al. 2017).

In the Cenozoic sedimentation and facies distribution were strongly affected by oceanographic processes and climatic changes (Light et al. 1993; Weigelt and Uenzelmann-Neben 2004). The early Oligocene opening of the Drake Passage in the south created the cooler Antarctic Circumpolar Current and Atlantic meridional overturning circulation currents leading to the subsequent development of thermally stratified bottom and deep-water currents in the Miocene (Weigelt and Uenzelmann-Neben 2004; Uenzelmann-Neben et al. 2017). Southern-sourced bottom and deep-water currents responsible for depositional changes observed since the Miocene offshore SW Africa include the Antarctic Intermediate Water current, North Atlantic Deep Water, and deep Antarctic Bottom Water currents, together with the Benguela Coastal Current (Weigelt and Uenzelmann-Neben 2004). These thermally stratified countercurrents led to cold water upwelling of the Benguela Current in the Miocene intensifying at ~ 11 Ma (Diester-Haass et al. 2004; Rommerskirchen et al. 2011).

The post-rift stratigraphy of the Orange Basin has been well-described and subdivided in terms of several stratigraphic units/sequences separated by key stratigraphic markers/bounding surfaces (e.g., Emery et al. 1975; Bolli et al. 1978; Brown et al. 1995; Holtar and Forsberg 2000; Paton et al. 2008; Granado et al. 2009; De Vera et al. 2010; Kuhlmann et al. 2010; Dalton et al. 2017; Baby et al. 2018; Maduna et al. 2022). Several phases of uplift and denudation in the post-rift succession have enhanced gravitational processes within the basin, responsible for both crustal thinning and the inversion of extensional faults (e.g., Granado et al. 2009; De Vera et al. 2010; Hirsch et al. 2010; Brown et al. 2014; Wildman et al. 2015). Periods of elevated sedimentation rates are recorded mostly in the Upper Cretaceous (93.5–66 Ma), then later in the Oligocene (~ 30–25 Ma) successions (Baby et al. 2020). Elevated sedimentary flux in the Upper Cretaceous corresponds to a major uplift of the South African Plateau (De Vera et al. 2010; Hirsch et al. 2010), caused either by a dynamic topography as the African plate moved over the African Superplume found in the lower mantle, or via lithospheric delamination/metasomatism (Baby et al. 2020). Gravitational collapse structures (DWFTB systems) found in the Orange Basin (Fig. 3) formed in response to this major margin uplift together with seaward tilting, significantly eroding the inner margin (Paton et al. 2008; Granado et al. 2009; Hirsch et al. 2010; De Vera et al. 2010; Kuhlmann et al. 2010).

Aptian-, Turonian- and Cenomanian-aged maximum flooding surfaces are seaward-dipping, over-pressured shale detachments upon which gravitational sliding of DWFTB systems occur in the Orange Basin (Brown et al. 1995; Morley et al. 2011; Dalton et al. 2015; Baby et al. 2018; Maduna et al. 2022). A full system consists of a linked: (1) up-dip extensional domain with listric normal faults separating convex-upward growth strata; (2) central transional (or trans-lational) domain with complex overprinted extensional and

compressional tectonics; and (3) down-dip compressional domain where folds and thrust faults occur (Fig. 3; Rowan et al. 2004; Bilotti and Shaw 2005; Morley et al. 2011). Toe thrusting and folding occurs within an approximately 3 km thick section extending for up to 60 km in the direction of transport in the compressional domain (Morley et al. 2011).

The study of DWFTB systems has grown because of their association with economic hydrocarbon reserves in the distal folds of anticlines (compressional domain); for example, the northern Orange Basin in Namibia (van der Spuy and Sayidini 2022) and the Niger Delta (Bilotti and Shaw 2005; Corredor et al. 2005; Krueger and Gilbert 2009).

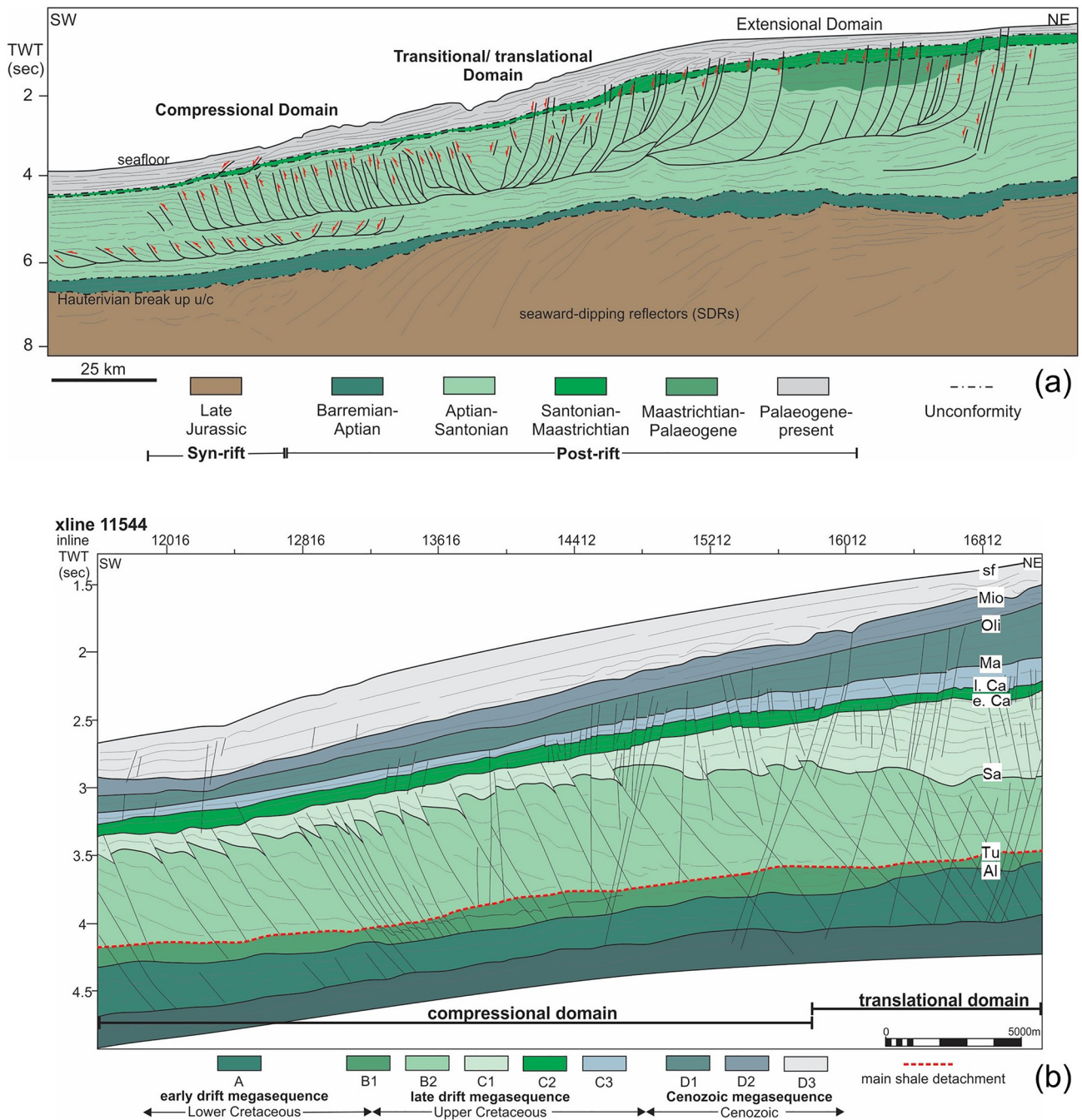


**Fig. 3** 2D seismic profiles through DWFTB systems of the Orange Basin showing; **a** a full DWFTB system comprised of an up-dip extensional, central transitional (or translational) and down-dip compressional domain (De Vera et al. 2010); and **b** the detailed translational

and compressional domains imaged in the present study area (Maduna et al. 2022). Abbreviations: *Al* Albian, *Tu* Turonian, *Sa* Santonian, *Ma* Maastrichtian, *e. Ca* early Campanian, *l. Ca* late Campanian, *Oli* Oligocene, *Mio* Miocene, and *sf* seafloor. Vertical exaggeration = 5

## Hydrocarbon system

Exploration in the shallow shelf environments of the Orange Basin has confirmed several petroleum systems sourced from Barremian to Albian, and possibly Turonian shales (Aldrich et al. 2003; van der Spuy 2003). The two commercial hydrocarbon plays in the shallow proximal settings of the South African basin are the Ithubesi gas field (Fig. 1) and A-J oil syn-rift system (van der Spuy and Sayidini 2022). The Ithubesi gas field is sourced from the lower Aptian source shales located in the depocentre of the Orange Basin with reservoirs stratigraphically trapped in fluvial channel-fill sandstones (PASA 2017). A similar gas play in the shallow shelf regions is the Kudu gas field, offshore southern Namibia (Fig. 1). The Kudu gas field is sourced from Barremian shales with reservoirs stratigraphically trapped within aeolian sandstones (PASA 2017). These plays both have the potential of multi-TCF (trillion cubic feet) natural gas reserves. The only oil system found in the shallow shelf region occurs within the isolated A-J half-graben sourced from rich Hauterivian lacustrine shales (Jungslager 1999). Oil reservoirs are stratigraphically trapped within lake shoreline sandstones interbedded within the source rocks (PASA 2017). Results from the DSDP 361 borehole and a possible Turonian oil source rock imaged the Bredasdorp Basin, indicates that the Orange Basin becomes increasing oil-prone distally (Fig. 1; van der Spuy 2003; PASA 2017). This is proven in Namibia as recent significant light oil discoveries were made from Shell's Graff-1 appraisal well and TotalEnergies' Venus-1X wildcat well drilled between 2 and 3 km water depths with reservoirs speculated to be located in the significantly older Aptian to lower Albian sediments (Fig. 1; Heins 2022; van der Spuy and Sayidini 2022). Currently, South Africa's largest deep-water prospect is found within the southern Outeniqua Basin's Brulpadda blocks, hosting an average of one billion BOE (barrel of oil equivalent) of natural gas condensate (Feder 2019). Due to the harsh conditions imposed by the setting of the strong Agulhas current, however, not much progress has been made in drilling (L'Arvor et al. 2020).

## Overview of natural gas/fluid escape features

The most well-known seafloor (or palaeo-seafloor) expressions of vertically focussed fluid flow in hydrocarbon systems include mud volcano systems and pockmarks. These surface expressions are linked to subsurface processes such as pipes and chimneys, formed within fracture zones, reflecting the focussed movement of gas, fluids and large sedimentary masses in the case of mud volcanoes (Mazzini and Etiope 2017).

## Surface expression of natural gas/fluid flow

Mud volcanoes, first recognised and described in the 1970s, are unstable topographical features formed by rapid rates of relative methane expulsion, with rates high enough to remobilize sediment and fluids to the surface (Roberts et al. 2006; Judd and Hovland 2007; Andresen 2012). Mud volcanoes episodically vent a mixture of gas (large amounts of hydrocarbon gas and methane, and lesser amounts of CO<sub>2</sub>, N<sub>2</sub> and He), oil, water, mud and rock fragments (constituents forming the mud breccia) in a process termed 'sedimentary volcanism' (Dimitriv 2002; Judd and Hovland 2007; Mazzini and Etiope 2017). Sedimentary volcanism is driven by the gravitative instability of buoyant shales and fluid overpressures, leading to hydrofracturing and the subsequent flow of fluids along permeable fractures (Mazzini and Etiope 2017). The most extensive mud volcanoes systems are found in the offshore environment since water-saturated conditions yield low viscosity flows (Mazzini and Etiope 2017). In compressional margins Judd and Hovland (2007) note that there is a relationship between earthquakes and mud volcanoes; a major earthquake may be triggered sedimentary volcanism, which may in turn trigger minor earthquakes. From satellite imagery and field observations, the distribution of mud volcanoes is shown to be often structurally controlled as they occur with normal faults, strike-slip faults, fault-related folds and along the axis of anticlines (Mazzini et al. 2009; Mazzini and Etiope 2017).

Pockmarks are elliptical or cone-shaped depressions in fine-grained sediment (Hovland and Judd 1988), and were first documented by King and MacLean (1970) on the Scotian shelf. Unlike the large vent feeding a mud volcano, the flux of gas-saturated mud in blowout pipes is moderate, and therefore insufficient to form a large edifice on the seafloor resulting in the formation of smaller pockmarks (Roberts et al. 2006; Cartwright 2007). The escape of fluids erupting to the surface is envisaged to be quite violent during the initial formation of pockmarks then followed by smaller seepages along the same migration pathway (Judd and Hovland 2007). The size of pockmarks varies depending on the grain size of sediments they are hosted in (Judd and Hovland 2007), and type and size of the underlying conduit. Numerous pockmarks have been described both in the shallow (Jungslager 1999; Kuhlman et al. 2010; Hartwig et al. 2012; Isiaka et al. 2017; Palan et al. 2020) and deep-water reaches (Mahlalela et al. 2021) of the Orange Basin on the palaeo-Cenozoic and current seafloors. In the shallow water reaches of the basin, seafloor pockmarks are associated with active faults (e.g., Jungslager 1999; Hartwig et al. 2012).



## Subsurface expression of natural gas/fluid flow

The gas and fluid pathways responsible for the surface expression of gas/fluid escape features are created by discontinuities and unconformities primarily in the form of faults, faulted anticlines, salt diapirs and structural surfaces along the bedrock (Gay et al. 2003). A type of faulting system above hydrocarbon reservoirs in fine-grained sediment are polygonal faults describing a honeycombed hydraulic fracturing pattern in planform (Henriet et al. 1991; Cartwright 1994, 2007). Polygonal faults are often linked to pockmark formation acting as fluid migration pathways (Cartwright et al. 2003; Gay et al. 2006, 2007). Polygonal faults are attributed to mechanisms such as differential compaction and dewatering, overpressures, density inversion and dissolution-induced shear failure (Cartwright et al. 2003; Cartwright 2007, 2011).

Seismic chimneys and pipes are the most common subsurface processes reflecting the vertical movement of gas/fluids through fracture systems to the surface (Løseth et al. 2011; Gay et al. 2006, 2007; Cartwright et al. 2007). Chimneys indicate slow methane expulsion rates, while smaller pipes which lead to surface pockmarks are indicative of moderate methane expulsion rates (Roberts et al. 2006). According to Andresen (2012), a chimney is defined as a wide (sometimes narrow) vertical zone of focussed fluid flow characterised by low amplitude, disrupted or chaotic reflectors; and a pipe is defined as a narrow (< 300 m) vertical zone of focussed fluid flow mainly characterised by stacked, high amplitude anomalous reflectors. There are many hypotheses when it comes to the formation of seismic pipes and chimneys, discussed in detail by Cartwright and Santamarina (2015). Hypotheses include hydraulic fracturing and erosive fluidization (Brown 1990; Løseth et al. 2009, 2011; Cartwright et al. 2007), capillary invasion (Cathles et al. 2010), localized subsurface volume loss similar to the formation of mud volcano pathways (Roberts et al. 2006) and syn-sedimentary formation (Cartwright and Santamarina 2015). The most popular hypothesis of pipe and chimney formations is hydraulic fracturing caused by the combined effects of elevated pore fluid pressures with fluid-driven erosion (Cartwright 2007). Other subsurface processes include mud intrusions and mounds, domes, dewatering pipes, domes, diapirs and diatremes; all of which are referred to as piercement structures by Mazzini and Etiope (2017).

## Data and methods

### Seismic acquisition, processing, and interpretation

Three deep-water 3D seismic surveys have been conducted in the deep-water extents of the South African Orange

Basin (van der Spuy and Sayidini 2022). The first acquired in 2002 exhibited low signal-to-noise ratio; then, between 2012 and 2014, two large, higher-resolution 3D seismic surveys were conducted. This present study uses a portion of the northern-most 3D seismic dataset bordering the Namibian maritime licensing region (Fig. 1). Shell Global Solutions International commissioned the present study's high-resolution 3D seismic survey between 2012 and 2013 (Kramer and Heck 2014). The survey was conducted in a ~ NNW to SSE orientation, covering a total area of ~ 8200 km<sup>2</sup> (Fig. 1b). However, in this study, we interpret the northernmost ~ 1800 km<sup>2</sup> portion of the full seismic dataset bordering Namibia.

Seismic acquisition was conducted onboard the *Dolphin Geophysical Polar Duchess* using the UTM Zone 33S, central meridian 15° map projection. The source used was an array of dual airguns 15 m in length with a separation of 100 m, volume of 4100 cubic inches, 25 m shot point interval (flip/flop) towed at 8 m depths. The group interval and group length for the 7950 m long streamers were both 12.5 m, with each of the 8 streamers being 7950 m in length, separated by 200 m. The data were recorded in SEG-D format with a record length of 7186 ms, sampled at a rate of 2 ms using a low-cut and high-cut frequency of 4.4 Hz at a 12 db/Oct slope and 214 Hz at a 341 db/Oct slope, respectively. Following pre-processing involving data conversion from SEG-D to SEG-Y output onboard the *Dolphin Geophysical Polar Duchess*, full seismic processing was carried out by the Netherlands Global Processing team using Shell's proprietary SIPMAP software. Processing was done at 4 ms from SEG-Y field tape data through surface-related multiple elimination (SRME) using 3D SRME and anisotropic Kirchhoff pre-stack depth migration (PSDM). The original acquisition grid for the inline and crossline was 6.25 m × 50 m, respectively. Following PSDM migration, the final crossline and inline cell size output is given as 25 × 25 m according to Shell's report for the study area (Kramer and Heck 2014). The full acquisition and step-by-step processing parameters are added as tables in the supplementary material.

In this study, the data are geologically interpreted using Schlumberger's Petrel software. The seismic data has a dominant frequency of 20 Hz and an average velocity of 2400 m/s (see Kuhlman et al. 2010). With a wavelength of 120 m, the vertical seismic resolution is calculated to be either 60 or 30 m based on the ½ and ¼ wavelength criteria, respectively (Yilmaz 2001). The horizontal resolution for migrated seismic data is defined by ½ the wavelength (i.e., 60 m for these data) (Herron 2011). However, this resolution is also dependent on the quality of the data, bin size or trace spacing and geometry of the survey (Lebedeva-Ivanova et al. 2018).



## Application of seismic attributes

Seismic attributes were applied to the seismic data to image features below the vertical and horizontal resolution limits as in Manzi et al. (2013) and Schoole et al. (2020). Volumetric attributes applied to the full seismic dataset prior to seismic interpretation include variance, generalized spectral decomposition (GSD), envelope, sweetness and the iterative root mean square (RMS) amplitude. Since seismic attributes are sensitive to noise, structural smoothing was first applied to the full seismic volume to precondition the data and enhance the signal-to-noise (S/N) ratio (Randen et al. 2000). Variance was then applied to the structurally smoothed dataset. Variance is an attribute that highlights discontinuities by measuring local deviations in the seismic signal through a coherency analysis (Silva et al. 2005; Maselli et al. 2019). Envelope is the most popular trace attribute used to detect hydrocarbons as it highlights acoustic impedance contrasts in sandstone reservoirs as bright spots (Koson et al. 2014). The RMS amplitude (iterative) and sweetness attributes are highly correlated to envelope and are therefore also used to detect 'bright spots' (i.e., possible hydrocarbon reservoirs). The RMS amplitude (iterative) is a smoother, scaled estimate of the trace envelope (Koson et al. 2014). It computes the root mean square (RMS) iteratively on instantaneous trace samples over a user-specified vertical window. The sweetness attribute, defined as envelope divided by the square root of instantaneous frequency, is often used to image coarse-grained sandstone reservoirs. GSD uses the concept of unravelling the seismic waveform back to its pre-computed waveforms and constituent frequencies (Chopra and Marfurt 2005; Koson et al. 2014). Tuning the seismic data to specific frequencies allows subtle changes in lithology or flow barriers to be detected (Chopra and Marfurt 2005). The GSD attribute is also used as a direct hydrocarbon indicator, known to show gas charged reservoirs (Burnett et al. 2003; Naseer et al. 2017). Horizon-based attributes were applied once sufficient seismic interpretation had taken place on surfaces of interest. These include the edge detection, and influential data attributes; structural operations applied to the seafloor and late Campanian surfaces to highlight 3D geometric variations introduced by fault displacements and gas/fluid escape features. Edge detection extracts an edge model to enhance discontinuities by combining the dip and dip azimuth properties and normalizing these to the local noise of the surface (Randen et al. 2000; Manzi et al. 2012). Influential data is essential to ensuring sensible geometric form as it enhances areas of rapid 3D geometric variation. Prior to edge detection and surface smoothing, however, surface smoothing was first applied to filter out anomalous peaks and noise on each surface.

## Seismic interpretation strategy

The seismic stratigraphy is described using Mitchum et al. (1977)'s classical approach whereby stratal termination patterns (downlap, onlap, toplap erosional truncation and concordance) separate the sedimentary succession into seismic facies or sequences with distinct internal reflection geometries (e.g., parallel, subparallel, divergent, prograding, chaotic, sigmoid, hummocky). The surfaces that separate these sequences are erosional or conformable stratigraphic markers created through the interaction of sedimentation and sea-level fluctuations as depositional regimes change (Caturanu 2006). The stratigraphic markers used in this study were chosen because of their dominant high amplitudes and lateral continuity observed throughout the seismic volume. Since no wells are present in the deep-water region, a direct well tie could not be performed on the dataset to calibrate the geological ages to the stratigraphy. Geological ages were assigned based on the comparison of previous Orange Basin studies with seismic data and well logs (e.g., Brown et al. 1995; de Vera et al. 2010; Kuhlmann et al. 2010; Hirsch et al. 2010; Baby et al. 2018). The stratigraphic markers identified in the Cretaceous are the Albian, Turonian, Santonian, early Campanian, late Campanian and Maastrichtian surfaces (Fig. 3b). According to the offshore stratigraphic nomenclature developed by PetroSA the stratigraphic markers in this study correspond to the 14At1, 15At1, possibly 16Dt, 17At1 and 22At1 unconformities, respectively (Fig. 2; Brown et al. 1995). In the Cenozoic succession we identified the Miocene and Oligocene erosional unconformities (Fig. 3b), which were also recognised by Baby et al. (2018). The sedimentary succession is subdivided into four megasequences (A–D) reflecting the three major phases of margin evolution early drift (A), late drift (B1–C3) and Cenozoic (D1–D3) (Fig. 3b) as in Dalton et al. (2017).

## Results and interpretations

This study's seismic volume images the up-dip transitional and down-dip compressional domains of a Upper Cretaceous DWFTB system and the overlying Cenozoic succession between 1000 and 2000 m below sea level (mbsl) (Figs. 1, 3b and 4). The evidence for fluid and natural gas seepage in the seismic volume includes polygonal faults, pockmarks, a HPAA anticline and a mud volcano, well imaged on the late Campanian surface (Fig. 4). The structural framework associated with all these gas/fluid escape features include a combination of thrust faults, normal faults and oblique-slip faults associated with the Upper Cretaceous DWFTB system (Fig. 3b). Influential data (using two different colour tables) and edge detection were two key horizon-based attributes

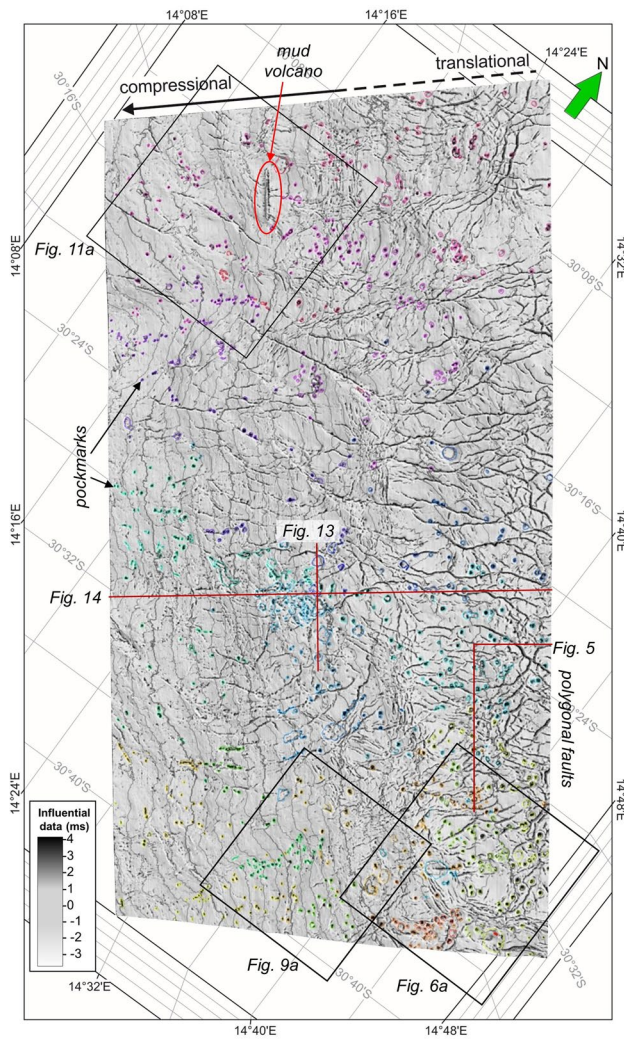


**Fig. 4** 3D late Campanian surface covering the full study area (Fig. 1) imaged with the influential data attribute (using a white–grey–black colour scale) to highlight features influencing the 3D form of the surface. The surface is highly pockmarked (pockmarks outlined by coloured polygons) with the greatest concentration of pockmarks occurring in the S (bottom left). Other features highlighted include polygonal faults in the E and SE, and an elongated mud volcano with few pockmarks surrounding it in the NW. Vertical exaggeration = 5

applied to better enhance all these features, together with the variance volumetric attribute enhancing discontinuities.

### Late Campanian pockmarks

There are over 950 well-preserved, elliptical-shaped depressions characteristic of pockmarks on the late Campanian surface (Fig. 4). The most efficient horizon-based attribute used to image these pockmarks clearly on the whole surface was influential data using a white–grey–black colour table (see Fig. 4). Late Campanian pockmark formation is strongly associated with

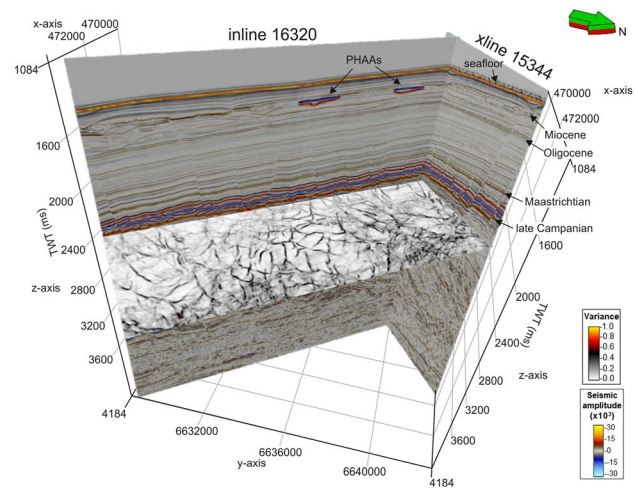


**Fig. 5** 3D view of an inline and crossline, together with the variance attribute timeslice (located just below the late Campanian surface) showing polygonal faults in cross section and their characteristic honey-combed pattern. PHAA positive high amplitude anomaly. Vertical exaggeration = 5

polygonal faulting in the eastern and southeastern sections of the study area, as many pockmarks of the surface are bound within them (Figs. 4, 5 and 6a). The variance time slice placed just above the translational domain of the Upper Cretaceous DWFTB system in Fig. 5 (south eastern portion of Fig. 4) displays the honey-combed pattern of polygonal faulting. Faults dip 45°, on average, and have variable dip directions accounting for the polygonal pattern seen in planform. Individual fault throws are 30–50 m and the distance between each fault (the size of each closed polygon cell) ranges from ~800 to 1200 m (Fig. 5). Most faults in the study area initiate from the Turonian shale detachment surface at depth and terminate around the late Campanian surface (Fig. 3b). Some of the faults in the eastern section of the study area, however, terminate at the Oligocene or Miocene surfaces (Cenozoic).

Pockmarks on the late Campanian surface were categorized into three different groups based primarily on their size and shape as: giant (8), crater (~20) and simple (>900) pockmarks. Giant pockmarks are greater than 1500 m in diameter with a ~1:16 depth-to-diameter ratio (Figs. 6 and 7). Crater pockmarks, named so because of their resemblance to simple crater meteorite impact structures, are mostly ~800 m in diameter with a 1:7 depth-to-diameter ratio. Crater pockmarks are linked to polygonal faults in the eastern section of the study area (Figs. 4, 5 and 6). Simple pockmarks are regular elliptical-shaped depressions with the smallest sizes (>500 m diameter and metre-scale deep). All the different types of pockmarks observed on the late Campanian surface are shown in Fig. 6 (a zoomed in portion of Fig. 4 in the SE). Figure 6a shows the association of different



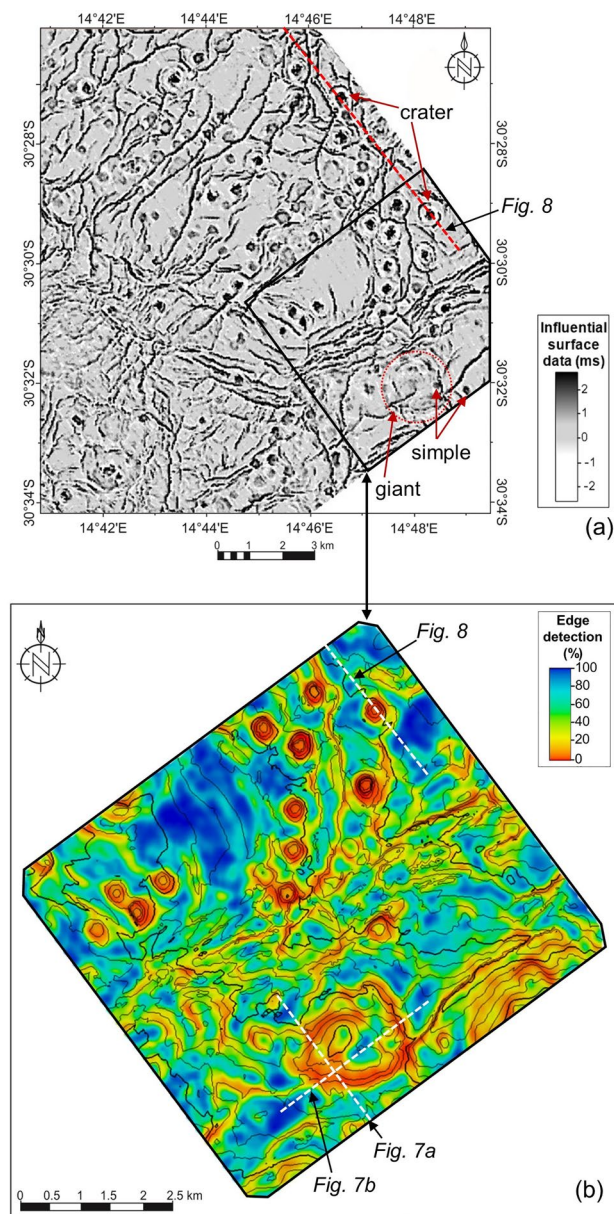


**Fig. 6** Different types of pockmarks on the late Campanian surface shown using: **a** the influential data attribute (using a contrast black to white colour table), and **b** the edge detection attribute on a zoomed in section

types of pockmarks to surrounding faults and fractures, and Fig. 6b is a close-up using the edge detection attribute.

Giant pockmarks are the largest pockmarks identified in the study, being 1500–2000 m in diameter (Figs. 6 and 7) and ~120 ms TWT (c. 114 m) deep (TWT-depth conversion using velocities of  $1900 \text{ m/s} \pm 10\%$ ; cf. Kuhlmann et al. 2010). There are a few (8) of these large, cone-shaped depressions throughout the study area (e.g., Fig. 6) often linked to wide chimneys at depth (Fig. 7a). An example of a giant pockmark is shown in Fig. 7. The inline in Fig. 7a

shows a large, dome-shaped anomaly of convex upwards deformed sediments leading up to the feature. This 1800 m wide zone of disrupted reflectors is a seismic chimney. The giant pockmark is bound between normal faults terminating above the Maastrichtian surface. Figure 7b, a crossline section, shows the pockmark's direct underlying stratigraphy is disrupted by normal faults. Smaller, simple pockmarks may occur within giant pockmarks as seen in Fig. 7b and the 3D image in Fig. 7c.

Pockmarks displaying a “crater-like” morphology in plan and cross-section (Figs. 6 and 8) are classified as crater pockmarks in this study. Crater pockmarks are 700–900 m in diameter (Fig. 6) and are approximately 120 ms TWT (c. 114 m) deep (TWT-depth conversion using velocities of  $1900 \text{ m/s} \pm 10\%$ ; cf. Kuhlmann et al. 2010). They have slightly raised wing-shaped rims giving them their distinctive “simple crater-like” morphology (Fig. 8b, c). Compared to giant pockmarks (Fig. 7) they are more circular in plan view (Fig. 6b) and symmetrical in cross-section (Fig. 8a, b). Crater pockmarks are confined to the SE region of polygonal faulting above the transitional domain (Fig. 6). The crater pockmarks are situated directly in the centre of polygonal fault cells (Figs. 6a and 8b). Intriguingly, these pockmarks are not associated with large zones of disrupted reflectors directly beneath them but appear to be related to faults and fracture zones (Fig. 8).

Simple pockmarks are much smaller in size, most are metre-scale in depth and less than 300 m in diameter, displaying elliptical- to cone-shaped morphologies (Figs. 7a, b and 9a). Furthermore, they lack the outer wing-shaped rims and are distributed throughout the late Campanian surface, unlike crater pockmarks which are confined to polygonal faulted areas above the translational domain (Figs. 4, 6 and 9a). Many simple pockmarks occur along faults (Fig. 6a), and others occur either randomly in between faults or follow a trend in seemingly un-faulted regions indicating possible microfractures (Fig. 9a). While giant pockmarks are linked to seismic chimneys at depth (Fig. 7), both crater and simple pockmarks are linked to faults at depth which are often difficult to distinguish (Figs. 8 and 9c, d). Pockmarks do not appear to be linked to any pipes at depth (Fig. 8a), however, this may be due to possible pipe widths being below the seismic resolution limit.

### Seafloor pockmarks and mass wasting

There are 85 pockmarks imaged on the seafloor with the greatest concentration occurring in the central and southern region of the study in the down-dip direction above compressional domain (Fig. 10). Seafloor pockmarks are similar to the late Campanian's simple pockmarks, although slightly larger in size, with most being ~400 m in diameter and less than 120 ms TWT (c. 114 m) deep (TWT-depth conversion

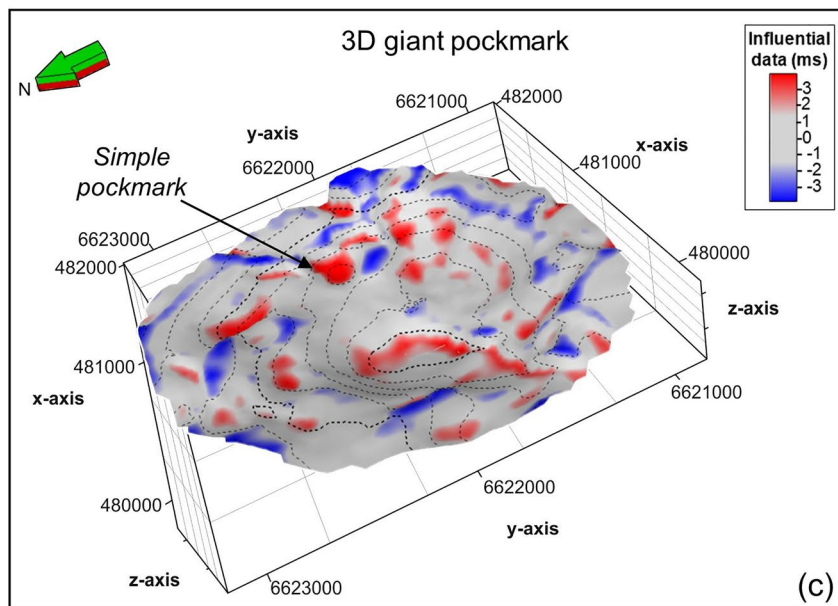
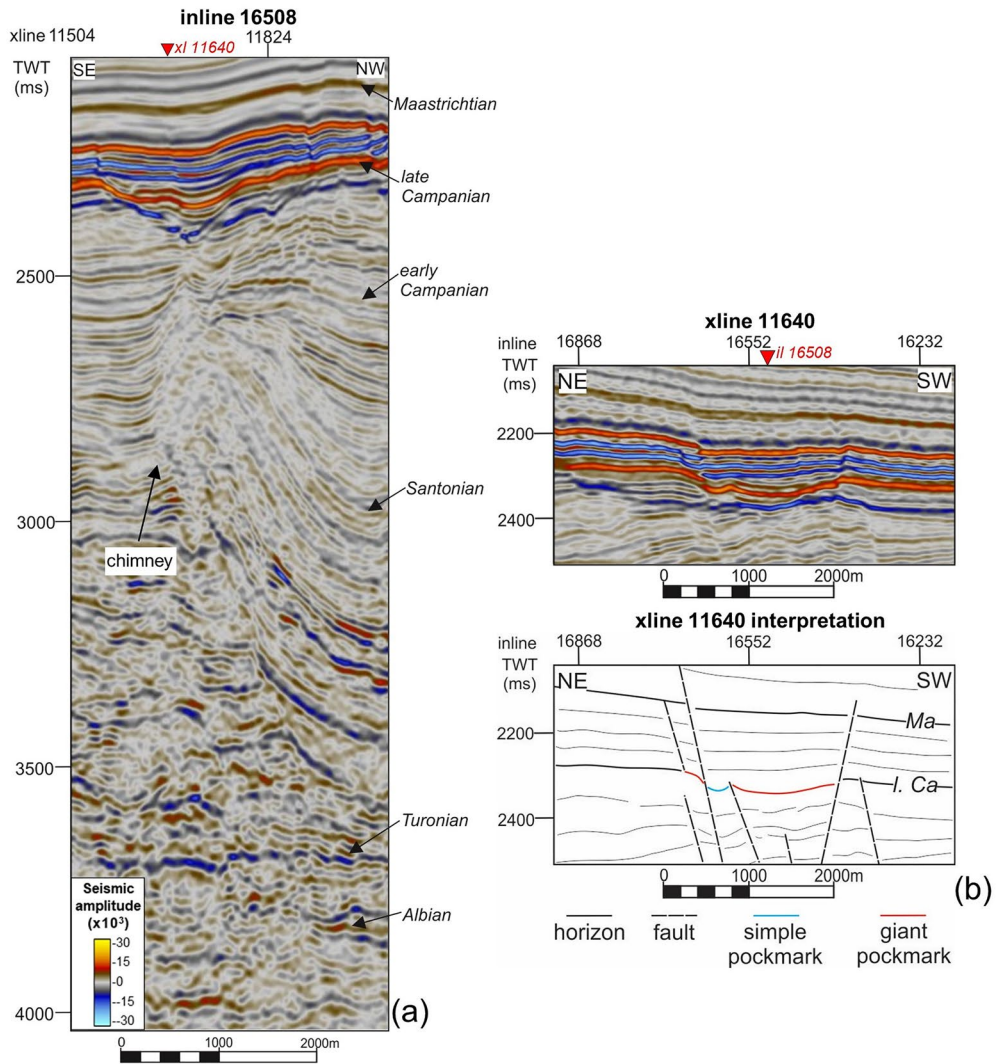




**Fig. 7** Example of a giant pockmark with a smaller, simple pockmark enclosed within it; **a** inline section showing a chimney leading up to the giant pockmark, **b** crossline section and interpretation of the giant and simple pockmark, **c** 3D influential data view of the giant and simple pockmark using the standard red-grey-blue colour scale. Vertical exaggeration = 5

using velocities of  $1900 \text{ m/s} \pm 10\%$ ; cf. Kuhlmann et al. 2010). Seafloor pockmarks are strongly influenced by the underlying stratigraphy with most occurring directly above those imaged on the late Campanian surface or following the same trend. An example of this is shown in Fig. 9a and b; fewer, larger pockmarks occur on the seafloor following the same NE-SW trend of those on the late Campanian surface. A conjoined simple pockmark pair on the late Campanian surface is shown to correspond to one large pockmark on the seafloor in the NW region of Fig. 9a and b. No other pockmarks are observed in the stratigraphy between the two surfaces, nor are there clearly distinguishable faults, pipes or chimneys leading up from the late Campanian to seafloor surfaces.

The only notable features observed between the late Campanian and seafloor surfaces, following the trend of both surfaces' pockmarks, are normal faults with some forming the sidewalls (gliding planes) of slides (Fig. 9c and d). The slides are coherent masses of sediment with little internal deformation. They are ~2–4 km in diameter with rotational slip occurring along the Miocene and Oligocene surfaces. In Fig. 9d original bedding planes are shown to have been rotated by the gliding plane of the slide. Some seafloor pockmarks are found within slides in the centre of the study area in the region directly above a late Campanian PHAA anticline (Fig.), and in the south (Figs. 9b, d and 10). Pockmarks associated with slides are larger in size (up to ~1500 m in diameter) and irregular in shape. The greatest mass wasting feature is seen in the NW; a large  $> 26 \times 19 \text{ km}$  slump scar characterised by low amplitude, internally deformed reflectors (Figs. 10, 11b and 12a, b). The slump scar is not associated with any pockmarks on the seafloor but with a mud volcano detailed in the following section (Figs. 11 and 12).

### Mud volcano

A NW–SE orientated topographical feature is found in the NW of the study area, with a positive relief of 50 ms TWT (c. 48 m) (TWT-depth conversion using velocities of  $1900 \text{ m/s} \pm 10\%$ ; cf. Kuhlmann et al. 2010), a length of ~4200 m, and width of ~400 m (Figs. 11 and 12). This

feature is interpreted as an elongated mud volcano. The mud volcano is located within the centre of a large, 7400 m wide anticline from the Upper Cretaceous DWFTB system (Fig. 11b, c). The anticline marks the intersection between the DWFTB system's compressional and translational domains. The mud volcano conduit roots from the Turonian surface as a wide ~1800 m zone displaying chaotic internal reflections which then narrows into an internally chaotic vent (Figs. 11b, c and 12). Deformation into convex-downwards layers, defining the positive relief of the mud volcano, starts just below the crest of the anticline in Santonian sediments (Fig. 11c).

On the late Campanian surface, the influential data surface attribute reveals a few simple pockmarks surrounding the mud volcano (Fig. 11a) which are not as densely populated as those found in the south of the study area (Figs. 4, 6 and 9a). The mud volcano is situated within a large, slumped region on the seafloor (Fig. 10). Within here, an even deeper depression (slumping within a slump) occurs to the SE, adjacent to the length of the mud volcano characterized by chaotic internal reflections from the Miocene to seafloor surfaces (Fig. 12a, b). Very few faults surround the mud volcano (Fig. 11a). Perpendicularly orientated fractures appear to feed into the mud volcano vent using the influential data surface attribute on the late Campanian surface, as presented in Fig. 11a. Figure 12 is an inline section that cuts through the length of the mud volcano. Reflections within the elongate vent are acoustically dampened and show low amplitudes compared to its surroundings in the envelope attribute (Fig. 12b).

### HPAA anticline

An anticline occurs along the late Campanian surface, appearing as an approximately 3.5 km (Fig. 13) by 4.2 km (Fig. 14) PHAA. The inline section presented in Fig. 13 shows the anticline is bound by faults dipping away from each other, depicting a horst structure. Four volume-based attributes known to detect the presence of hydrocarbons were used; iterative RMS, sweetness, generalized spectral decomposition (GSD) and envelope (Fig. 13a–d). The envelope attribute (Fig. 13d) best illustrated the presence of hydrocarbons with minimal loss in distinguishing strong reflections (surfaces and faults). Figure 14 shows the intersecting crossline section both normally (a) and using the envelope attribute (b) detecting the PHAA of the anticline and the overall interpretation (c). The outer edge from the crest of the anticline is likely the hydrocarbon spoil point which is bound by a fault (Fig. 14).

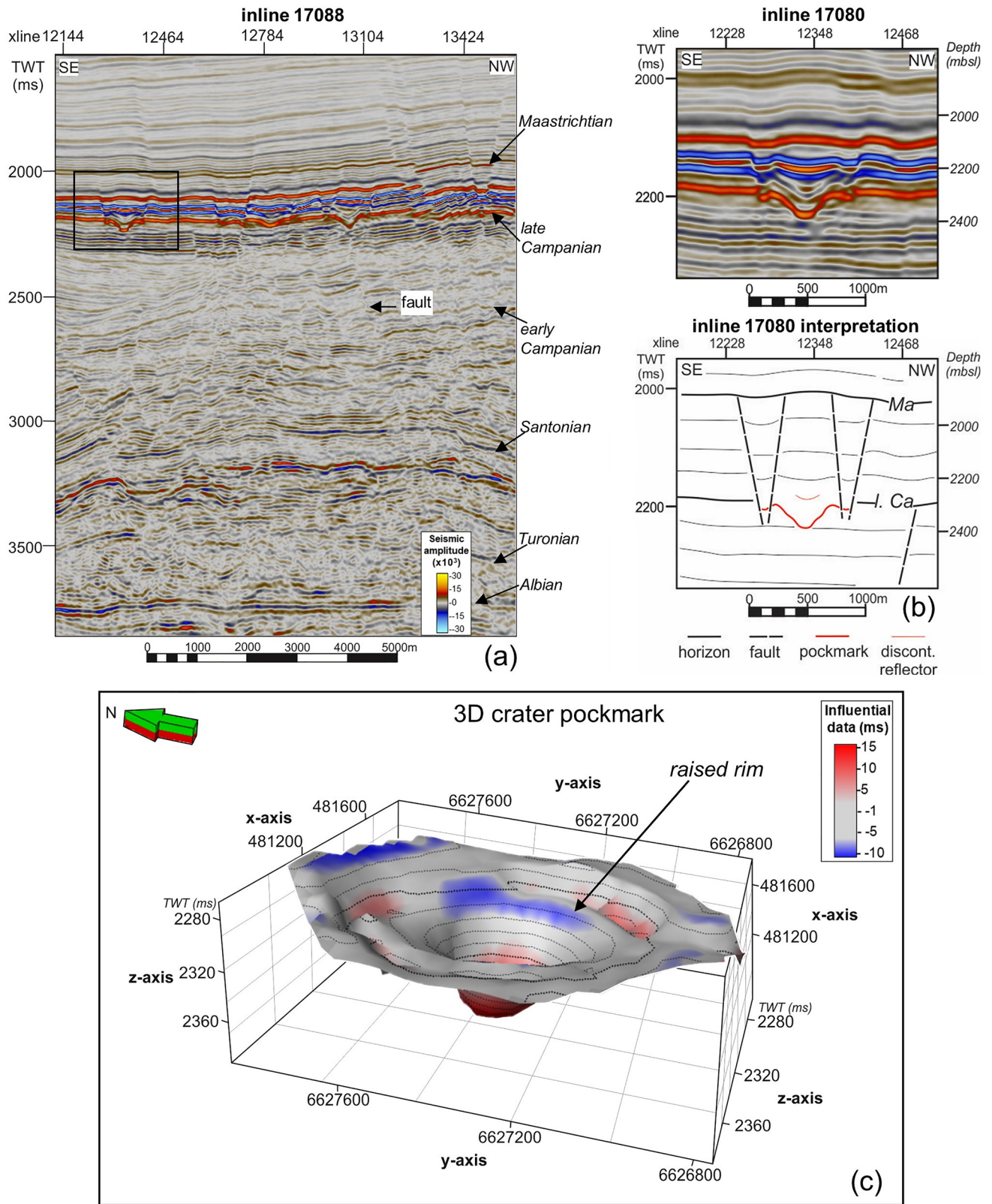


**Fig. 8** Example of a crater-type pockmark; **a** inline section showing two crater pockmarks with one clearly showing a fault leading up to it, **b** zoomed-in inline section and interpretation of a crater pockmark,

**c** 3D influential data view of the crater pockmark using the standard red–grey–blue colour scale. Vertical exaggeration = 3

Like the previously described mud volcano (Fig. 11), the anticline located further S occurs at the intersection of the translational and compressional domains of an underlying Upper Cretaceous DWFTB system (Fig. 14). In the region directly above the anticline, large pockmarks and slumps occur on the seafloor, as shown in Fig. 10. Pockmarks also occur along Campanian surface along the anticline but are difficult to see as they are highly irregular in shape (Fig. 4), deviating from the regular elliptical shape. PHAAs are also found within the Turonian to Santonian sediments in the region immediately below the anticline (Figs. 13 and 14). Up-dip of the anticline in the NE section of the study, the seismic character of the late Campanian to Maastrichtian sediments becomes progressively higher in amplitude, resulting in another PHAA above the translational domain as shown in Fig. 14b.

Most faults initiate from the Turonian surface in the compressional domain which often merges with the Albian surface in the translational domain (Fig. 14c). Thrust faults in the compressional domain terminate at the early Campanian to late Campanian surfaces, while many normal and oblique slip faults from the translational domain terminate along the stratigraphically younger Maastrichtian, Oligocene and Miocene sequence boundaries (Fig. 14c). Many smaller faults begin within early Campanian to late Campanian sediments in the translational domain and terminate in Cenozoic sediments (Fig. 14c).

## Discussion

The study of natural gas/fluid flow features is an underutilized tool in basin analysis that may explain various aspects of basin evolution including the timing of formation, main driving and trigger mechanisms, fluid source and migration pathways (Andresen 2012). Since the sedimentary succession is undisrupted by salt tectonics, the accumulation and distribution of hydrocarbons in the deep-water Orange Basin can be investigated. Gas/fluid escape features have been classified in several ways according to their geometry, lithology, surrounding geological impact, cause of formation or methane flux intensity (Roberts et al. 2006; Cartwright et al. 2007; Løseth et al. 2009; Huuse et al. 2010; Andresen 2012). The natural gas/fluid migration features observed in the study area include fluid migration conduits of faults and chimneys, and their surface expression as pockmarks, and a mud volcano on the late Campanian and seafloor surfaces. All these features are strongly controlled by

a Upper Cretaceous DWFTB system above or within which they occur (Maduna et al. 2022). The processes responsible for forming these gas/fluid escape features are based on the same common principles with one feature forming instead of another due to minor or major differences in influential factors such as the stress environment, sediment and fluid type, fluid concentration, or the influence of external triggers (Judd and Hovland 2007).

## Upper Cretaceous DWFTB system

Only the up-dip translational and down-dip compressional domains are imaged in the seismic dataset, with gravitational sliding having occurred along a main overpressurized Turonian shale detachment surface (Fig. 3b). The compressional domain is characterized by fold and thrust belts recognized throughout the Orange Basin (Figs. 1 and 3) along the continental slope in many studies (e.g., Paton et al. 2008; de Vera et al. 2010; Scarselli et al. 2016; Mahlalela et al. 2021). The previously ill-defined translational domain is characterized by overprinted extensional (listric normal faults) and compressional (thrust faults) tectonics with the downslope translation of sediment accommodated by extensive oblique-slip faults segmenting thrust sheets along strike (Maduna et al. 2022). Known and postulated source rock intervals of the Orange Basin include the Hauterivian, Barremian, Aptian and Turonian shales (Fig. 2). The Turonian shale detachment surface is the youngest and most speculative source rock interval estimated to have reached oil and gas maturation between 85 and 16 Ma with temperatures ranging between 100 and 140 °C along the shelf (Hirsch et al. 2010). Results from well logs and basin modelling suggest oil maturation in the deep water where sediment is thickest (Aldrich et al. 2003; van der Spuy 2003; Paton et al. 2008; Hirsch et al. 2010; van der Spuy and Sayidini 2022). The widespread occurrence of subsurface and surface gas/fluid escape features serves as indirect evidence of elevated pore fluid pressures in the Upper Cretaceous. Fluid overpressures are mainly formed by the combined effects of volumetric expansion involved in hydrocarbon generation and maturation, tectonic stresses and disequilibrium compaction (Rowan et al. 2004; Bilotti and Shaw 2005). Other mechanisms include mechanical compaction (due to sudden mass movement events or gradual burial), dehydration reactions and the thermal effect of increasing temperature gradients in pore fluids (Mazzini and Etiope 2017).



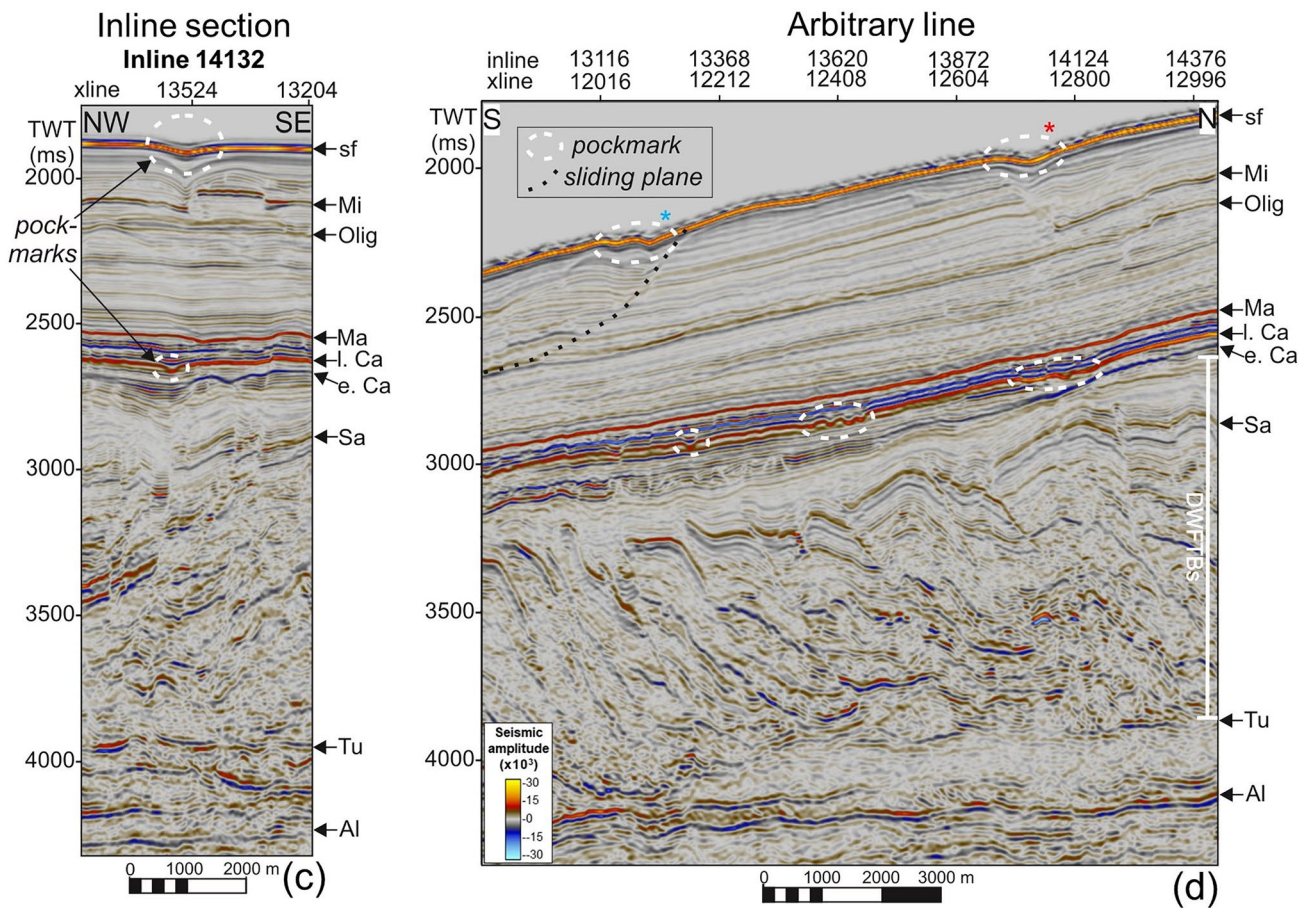
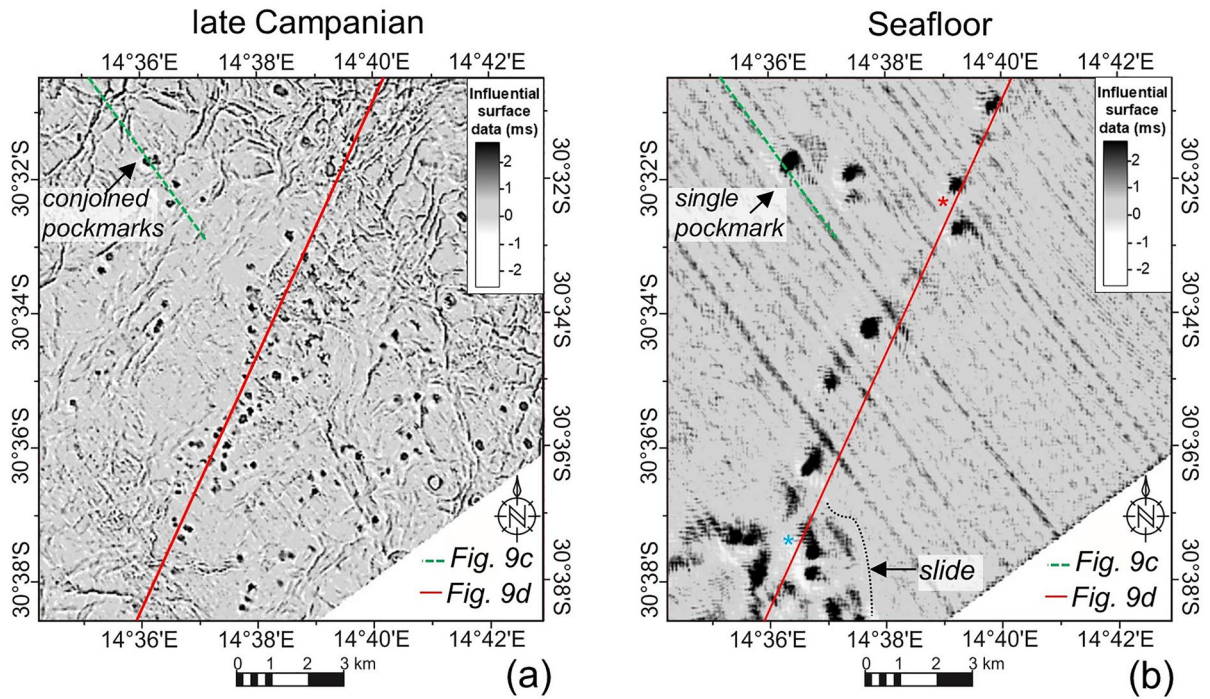




**Fig. 9** Comparison of the **a** late Campanian and **b** seafloor surface's simple pockmarks using the influential data attribute. In **c** an inline section is shown cutting through a pair of conjoined pockmarks on the late Campanian surface corresponding to a single pockmark on the seafloor. In **d**) an arbitrary seismic line following the linear trend of the late Campanian and seafloor pockmarks is imaged, showing the structure between the two surfaces and the underlying DWFTBs in the compressional domain. Abbreviations: *Al* Albian, *Tu* Turonian, *Sa* Santonian, *Ma* Maastrichtian, *e. Ca* early Campanian, *l. Ca* late Campanian, *Oli* Oligocene, *Mio* Miocene, and *sf* seafloor. Vertical exaggeration = 5

The distribution of all subsurface and surface gas/fluid escape features in this study are strongly influenced by the underlying tectonics of the Upper Cretaceous DWFTB system. Most of the fluid migration pathways linked to pockmarks on the late Campanian surface originate from the Turonian shale detachment surface (Figs. 7, 8, 9 and 12). Polygonal faults and crater pockmarks on the late Campanian surface are confined in the SW region above the translational domain (Figs. 4, 5 and 6). Simple pockmarks on the late Campanian and seafloor surfaces are concentrated above the compressional domain (Figs. 4, 9 and 10). At the intersection of the translational and compressional domains, a late Campanian PHAA anticline is found in the center of the study together with irregular seafloor pockmarks in the area directly above it (Figs. 10, 13 and 14). The orientation and location of the elongated mud volcano in the NW also occurs at the intersection of the two domains (Fig. 13b).

## Surface gas/fluid escape features

### Pockmarks

According to Judd and Hovland (2007), the density of pockmarks is dependent on the thickness, strength and permeability of the surrounding sediments. The overall distribution of pockmarks in the N of the study area are not as dense as those in the S for both the late Campanian and seafloor surfaces (Figs. 4 and 10). This implies low permeabilities, meaning fewer migration pathways resulting in the sparse distribution of pockmarks in the north compared to the south of the study area. Pockmarks in the deep-water study have been influenced by faults and chimneys leading up to the late Campanian and seafloor surfaces. On the late Campanian surface, wide chimneys are linked to giant pockmarks (Fig. 7a), and faults are linked to simple and crater pockmarks (Figs. 8a and 9c, d). All pockmarks are associated with bright(er) spots within the already high amplitude

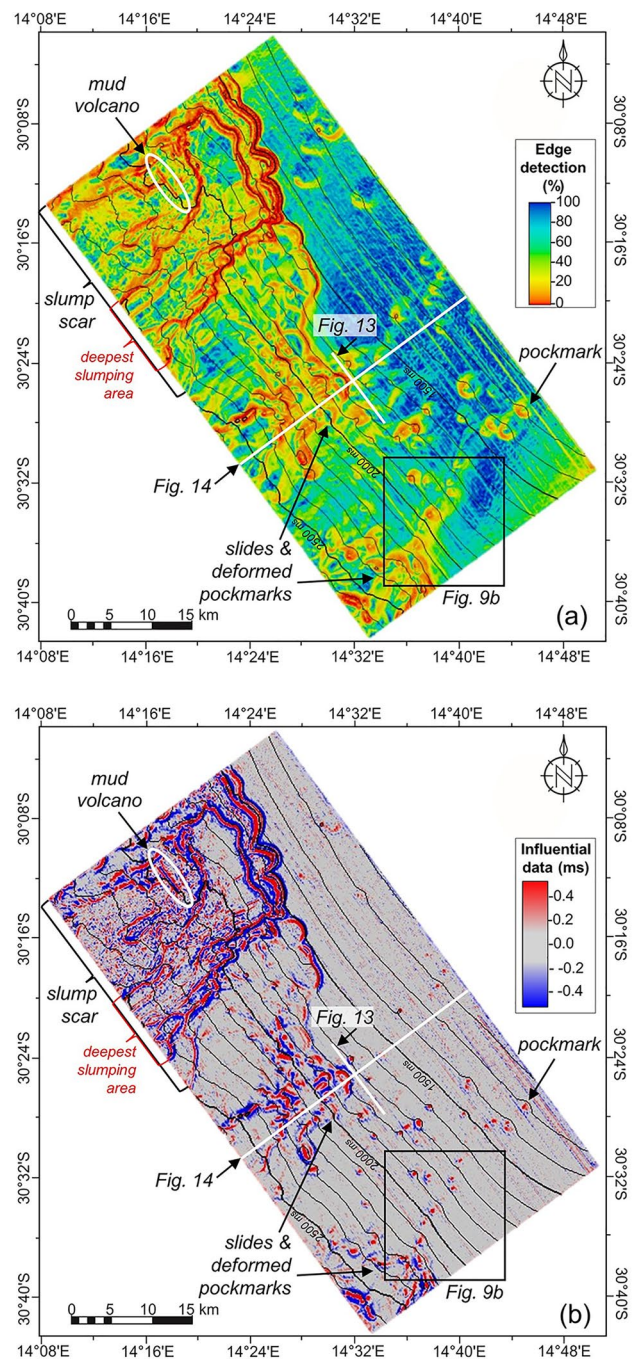


**Fig. 10** Pockmarks and slumping features on the seafloor imaged using **a** the edge detection, and **b** influential surface data attributes. The greatest concentration of pockmarks occurs in the S and is often associated with slides (e.g., Fig. 9). The NW is dominated by a large slump scar and within the feature an elongated mud volcano outcrops to the surface

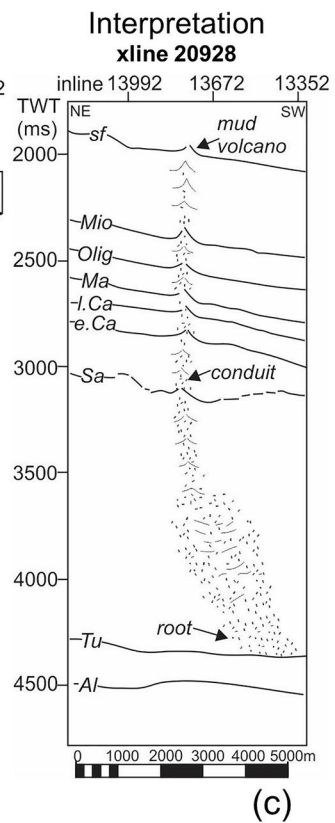
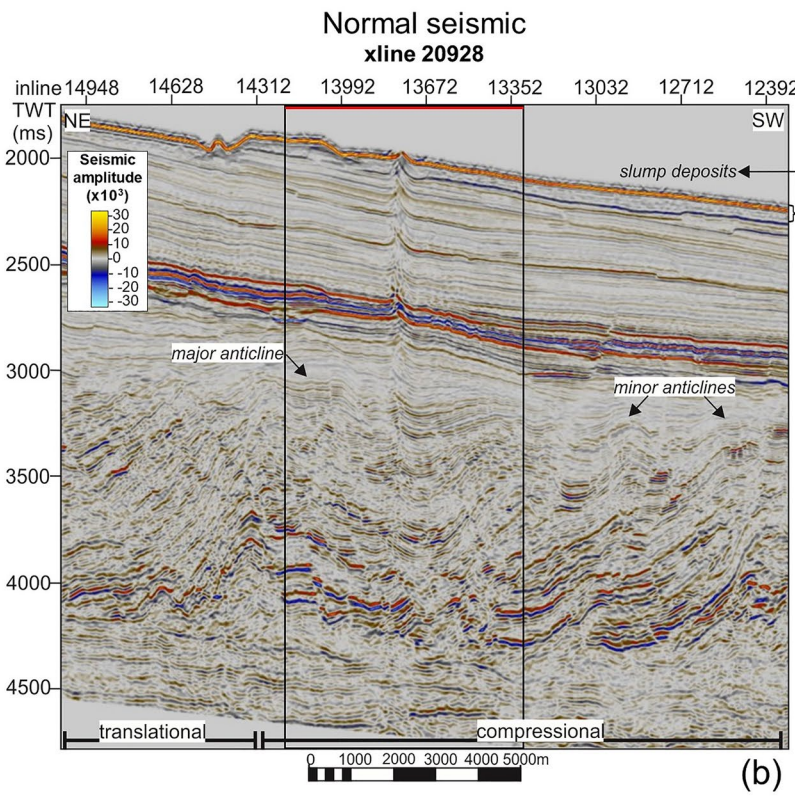
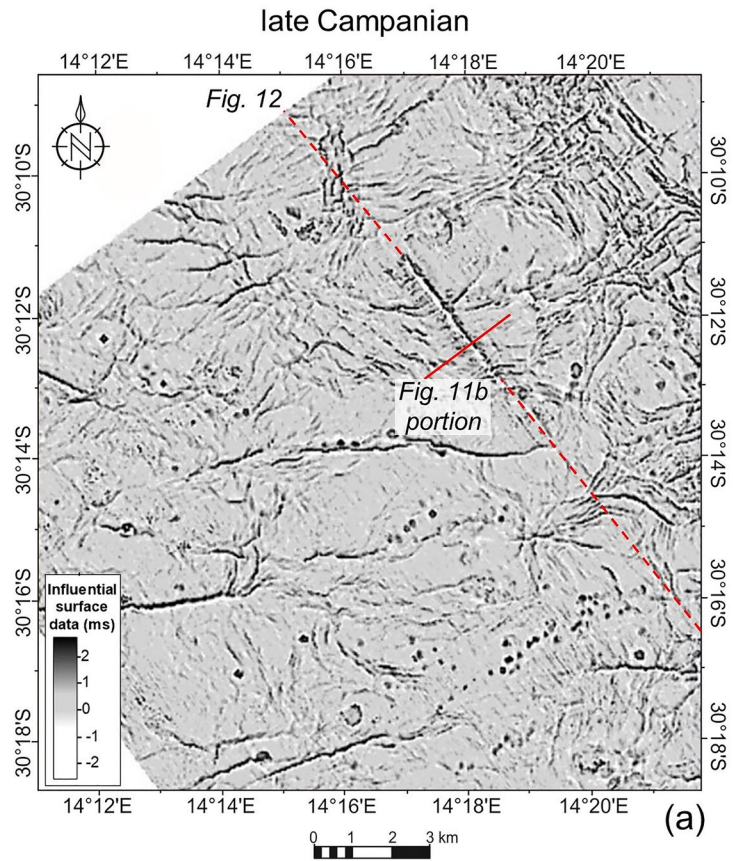




**Fig. 11** Mud volcano system. The location of the elongated mud volcano is shown on the late Campanian surface in (a) surrounded by simple pockmarks (red solid line = xline position shown in b and c; red stippled line = inline position shown in Fig. 12). The cross-section width of the mud volcano is shown in (b) situated in the centre of the largest anticline around the intersection of the translational and compressional domains. The interpretation of the mud volcano plumbing system along its width is shown in (c)

late Campanian and seafloor surfaces they are found along. Although the cross sections in Fig. 9c and d do not show a distinct association between the two pockmarked surfaces, the fact that seafloor pockmarks occur in the same area or follow the same trend as those of the late Campanian mean that there is a relationship. A possible explanation is that a

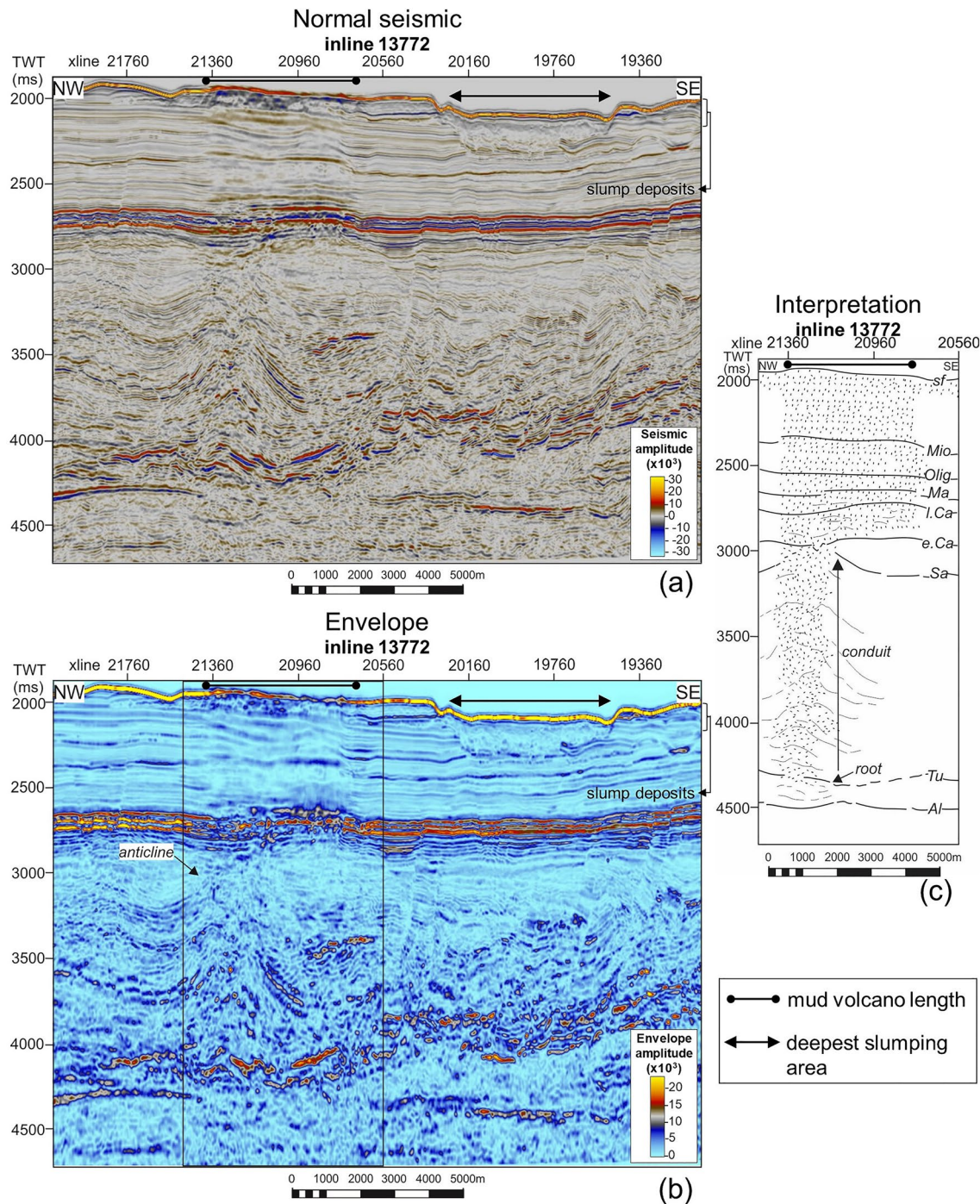


**Fig. 12** Mud volcano system and slump scar. The cross-section length of an elongated mud volcano is shown in (a) situated in the centre of the largest anticline with a major slump scar adjacent to it. The envelope attribute in (b) shows acoustically dampened and disrupted

reflections within the mud volcano system and the slump deposit compared to their surroundings. The interpretation of the mud volcano plumbing system along its length is shown in (c)



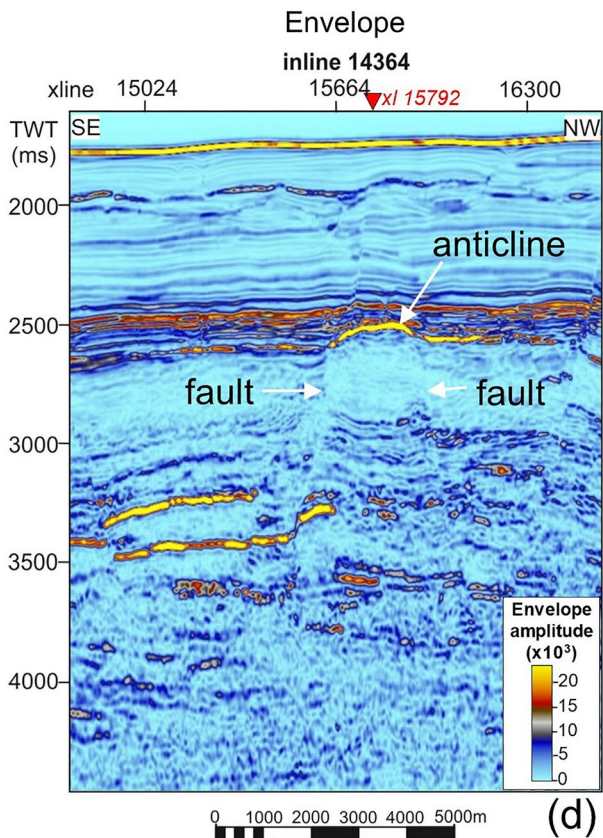
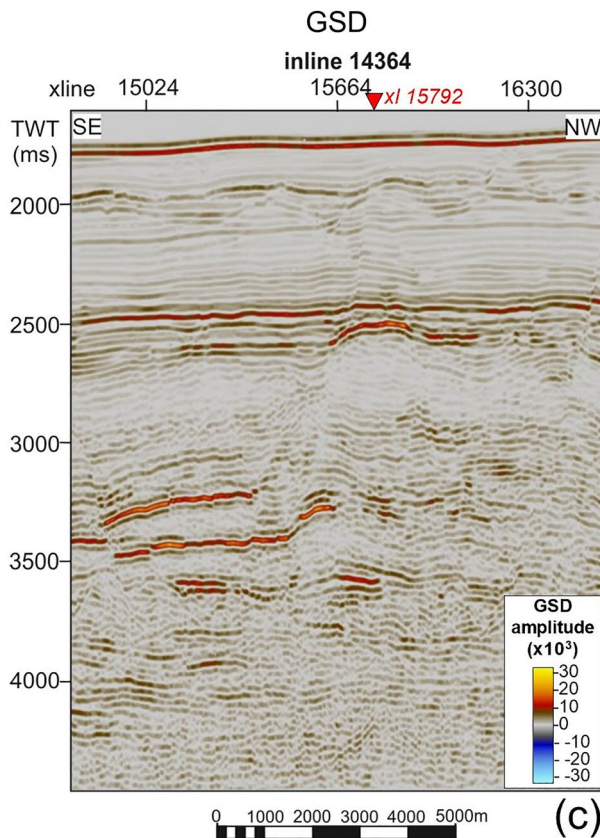
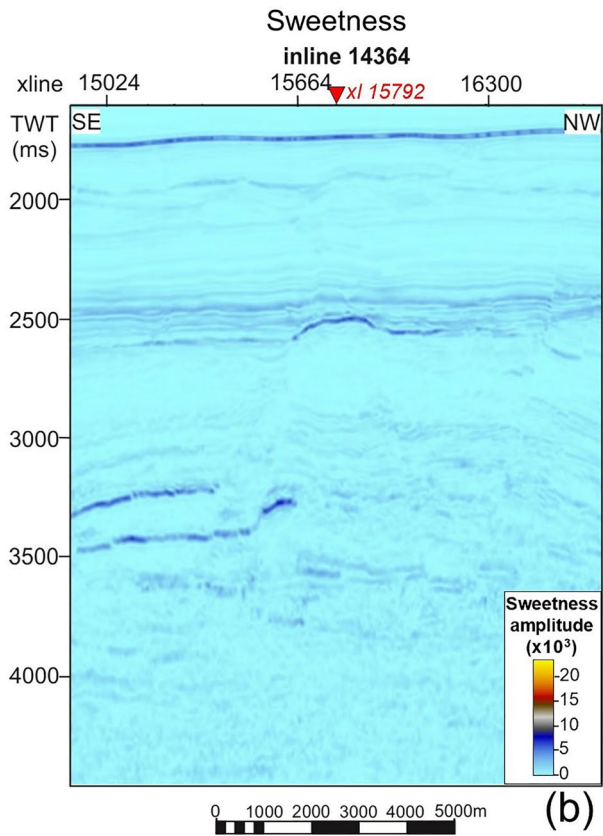
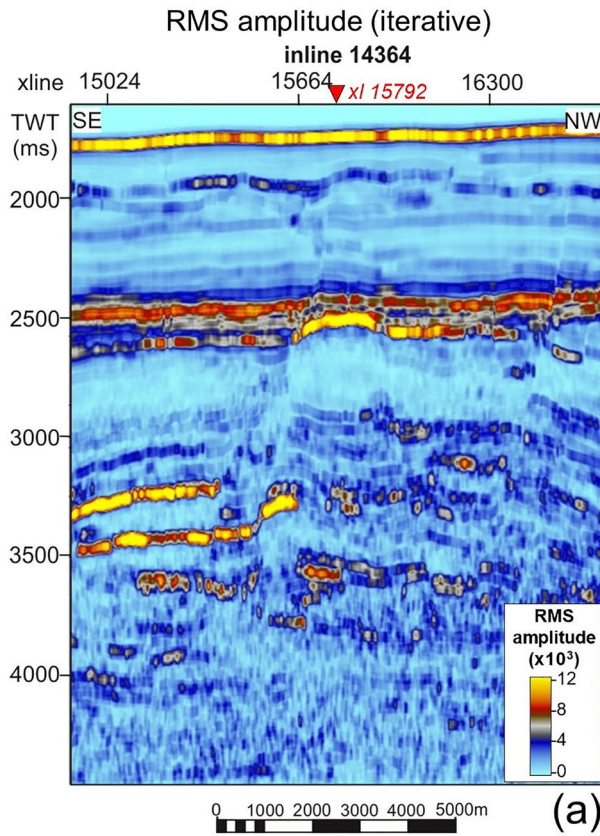




**Fig. 13** Inline section of an anticline located within a horst structure shown using the: **a** RMS (iterative), **b** sweetness, **c** GSD and **d** envelope volumetric attributes. Although all volumetric attributes used indicate the presence and accumulation of hydrocarbons along the high amplitude feature, the envelope volumetric attribute in (**d**) highlights the anticline well without distorting the stratigraphy and structure of its surroundings compared to other volumetric attributes

fracture system is at play, with displacements being below the smallest vertical resolution limit of 30 m between the two surfaces and below the late Campanian. A few giant pockmarks have also identified in the Barents Sea associated with melting ice, and three in the North Sea with one being the approximate size of a football field (900 m wide and 450 m deep) (Judd et al. 1994; Judd and Hovland 2007). Judd and Hovland (2007) attribute the formation of these giant pockmarks to the process of explosive decompression, whereby high fluid overpressures penetrate the surface in extreme cases such as the elongated Lokbatan-type mud volcanoes. Since giant pockmarks indicate rapid rates of methane expulsion (Roberts et al. 2006; Judd and Hovland 2007), so are their connected subsurface chimneys (Fig. 7).

Crater pockmarks are confined to the SE, located centrally within cells of polygonal faults (Figs. 4 and 6). Polygonal faults are found between the Santonian to Miocene sediments, have variable strike orientations, small fault throws and lateral extensions, and high densities (Figs. 4, 5 and 6). The variable strike orientations indicate that they do not have a principal stress direction (Fig. 5) and were thus not formed by regional compressional or extensional tectonics, but rather hydraulic fracturing (Cartwright 2007). Andresen and Huuse (2011) informally termed pockmarks associated with polygonal faulting as ‘bulls-eye’ pockmarks because of their central location within the faults. These ‘bulls-eye’ pockmarks are found within Plio-Pleistocene sediments of the Lower Congo Basin and have large size ranges, measuring between 70 and 500 m in diameter and 20–50 m in depth. In contrast to the ones observed on the Late Campanian surface in this study, those of the Congo Basin occur as a stacked succession in the stratigraphy. The concentric arrangement of pockmarks within, rather than above, polygonal faults strongly suggests that crater pockmark formation predates polygonal faulting (Andresen and Huuse 2011).

On the late Campanian surface, simple pockmarks dominate in the SW to NW compressional domain region, occurring along faults, in linear belts unrelated to visible faults and conjoined composite clusters (Fig. 9a), within giant pockmarks (Figs. 6, 7b and 11a), and otherwise random distributions (Fig. 4). The few pockmarks observed on the seafloor have a strong spatial relationship to those on the late Campanian surface with most displaying a simple circular morphology in plan view (Figs. 9a, b and 10). Directly south of the present study, Mahlalela et al. (2021) describe a few simple pockmarks on the seafloor that are 700–1100 m in

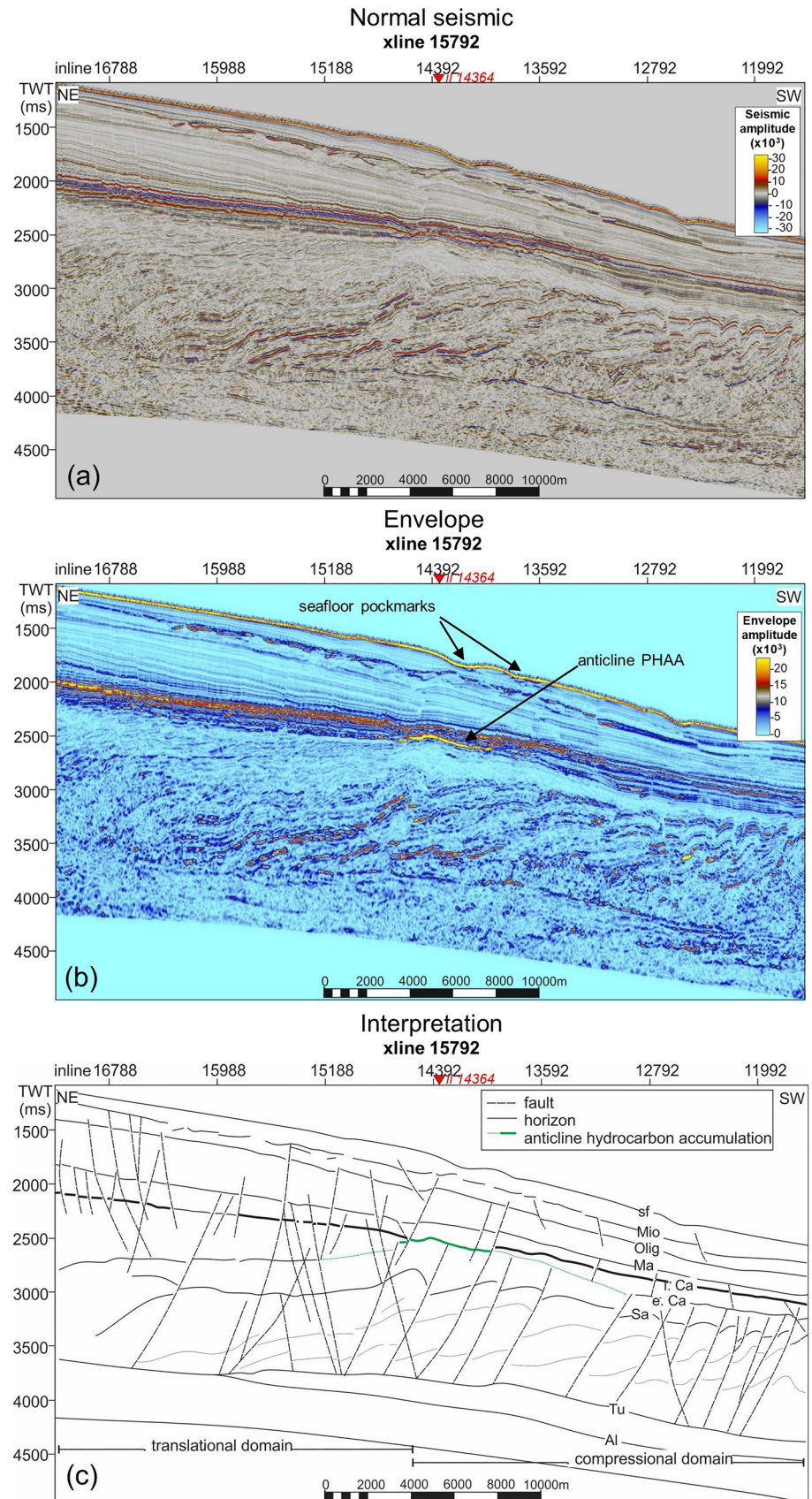
diameter with depressions 75–103 m deep. These pockmarks represent the same pockmark field observed on the seafloor surface in this study.

### Mud volcano

The morphology of mud volcanoes is controlled by several dynamic and mechanical factors, including: the frequency and vigour of volcanism, width of the conduit, pre-existing local topography, erosion type (e.g., bottom currents, wind, rain), rate of basin subsidence and the thickness and character of the affected strata (Mazzini and Etiope 2017). Cone-shaped mud volcanoes, the most common morphology, are observed in the shallow reaches of the Orange Basin following a N/NNW trend which is strongly associated with active, near-vertical strike-slip faults, thus reflecting neo-tectonic activity (Ben-Avraham et al. 2002; Viola et al. 2005). According to Viola et al. (2005) the mud volcanoes are the offshore structural expression of the same stress field observed onshore Namaqualand, South Africa and central Namibia, where recent faulting created N/NNW and NW orientated lineaments. Both offshore and onshore structures follow the present-day stress field of SW Africa and are thus postulated to be attributed to the Wegener stress anomaly (since the greatest horizontal compressive stress is NW/NNW). The mud volcano observed in this deep-water study also trends NW, however, unlike those observed in the proximal Orange Basin, it is elongated in morphology. An onshore example of an elongated mud volcano is the Lokbatan located in Azerbaijan (Planke et al. 2003; Mazzini and Etiope 2017). The Lokbatan has provided the basis of what is known of elongated mud volcanoes worldwide since it is easily accessible. This elongated mud volcano is characterised by extremely explosive eruptions with the last recorded in 2001 ejecting mud breccia after a large initial burst of hot methane (Planke et al. 2003; Mazzini and Etiope 2017). The volume of the Lokbatan mud volcano is affected by the deflation of the underlying shallow chamber following each eruption (Planke et al. 2003).

In like manner as the Lokbatan mud volcano coinciding with the trend of an anticline axis (Mazzini and Etiope 2017), the elongated mud volcano in this study is also situated along the axis of a deep-seated anticline (Fig. 11b, c) and is therefore tectonically controlled. The anticline forms part of a Upper Cretaceous fold and thrust belt marking the intersection of the translational and down-dip compressional domains. Sedimentary volcanism is postulated to have begun in the Santonian (86–83 Ma) since deformation shown by convex pull-up reflectors starts within these sediments (Figs. 11 and 12). This age coincides with the start of the oil and gas maturation window at 85 Ma estimated by Hirsch et al. (2010) for the Turonian shale detachment surface from which the mud volcano roots from (Figs. 11 and

**Fig. 14** Crossline section showing the stratigraphy and structure of the margin from an Upper Cretaceous DWFTB system underneath younger Cenozoic successions. The uninterpreted seismic section is shown in (a). The envelope volumetric attribute shown in (b) highlights the greatest accumulation of hydrocarbons as a PHAA defining an anticline, and c is the overall combined interpretation of the inline





12). The mud volcano gradually increased in height shown by stratigraphic surfaces leading up to the seafloor which could possibly indicate intense eruptions.

### Source of hydrocarbons

Since pockmarks and mud volcanoes are found in a wide variety of settings, from passive to active margin settings, in compressional zones such as accretionary prisms, fold and thrust belt systems, deltaic settings and deep sedimentary basins related to active plate margins (e.g., Judd and Hovland 1988; Gay et al. 2003, 2006, 2007; Loncke et al. 2004; Hustoft et al. 2010; Andresen and Huuse 2011; Ho et al. 2012; Hartwig et al. 2012; Anka et al. 2014), the source of their hydrocarbon system varies greatly. From the synthesis of past studies in the shallow Orange Basin (Jungslager 1999; Ben-Avraham et al. 2002; Kuhlmann et al. 2010; Hartwig et al. 2012), we postulate the source of hydrocarbons in this study to also be of both thermogenic and biogenic (or microbial) origin. According to van der Spuy (2003) and Paton et al. (2007), thermogenic gas originates from the deep, thermally mature Aptian source shales which become progressively oil-prone distally (Jungslager 1999). Since the Turonian shale detachment surface is also a speculated source rock interval, thermogenic hydrocarbons may have been sourced from both the deep-seated Aptian (unobserved in this study) and Turonian shales in this study. Fluid migration pathways stemming from the Turonian surface, together with late Campanian pockmarks linked to them, may therefore consist of thermogenic hydrocarbons. Biogenic gas is believed to originate from younger, organic-rich sediments involved in the upwelling of the Benguela Current in the Cenozoic (Kuhlmann et al. 2010).

An increase in biogenic activity attributed to the Benguela current upwelling system is recorded in the late Miocene to early Pliocene sediments offshore SW Africa (Diester-Haass et al. 2004; Rommerskirchen et al. 2011). This period of upwelling coincides with the development of thermally stratified bottom and deep-water currents offshore SW Africa resulting in major depositional changes observed in the Miocene (Weigelt and Uenzelmann-Neben 2004; Maduna et al. 2022). Seafloor pockmarks in this study are postulated to consist of a mixture of both thermogenic and biogenic hydrocarbons since the faults feeding them initiate from within the Cenozoic sediments; at the Oligocene and Miocene surfaces (Fig. 9c, d). The dissociation of gas hydrates is another possible origin for the source of hydrocarbons. Ben-Avraham et al. (2002) related their mud volcanoes in the shallower extents of the Orange Basin to a gas hydrate stability zone (GHSTZ) at depth. There is no evidence to support this hypothesis in the present deep-water study since no bottom-simulating reflectors (BSR) or other definitive gas hydrate indicators are observed in the seismic volume.

### Migration and accumulation of hydrocarbons

The distribution of surface and subsurface gas/fluid escape features shows the overall intensification of methane flux increases from the SE to the NW. In the SE, crater pockmarks on the late Campanian surface are associated with faults (moderate methane flux) (Figs. 4 and 6). In the NW, an elongated mud volcano (high methane flux) is found surrounded by a large slump scar on the seafloor (Figs. 4 and 10). Unlike the heavily faulted E, SE and central areas of the study, the NW has very few faults (Fig. 4). Consequently, instead of fluid flow pressures being distributed along many faults, one near-vertical fault-turned-vent took all the pressure, erupting gas, fluids and sediment to the palaeo- and current seafloors through an elongated mud volcano. Gas and fluids are postulated to have been escaping to the ocean/atmosphere since the Santonian when sedimentary volcanism began which may account for the lack of PHAAs within or surrounding the mud volcano (Figs. 11b and 12b). PHAAs are mostly found in the central and SW regions of the study (Figs. 5, 13 and 14). In addition to migrating upwards along fault surfaces, over-pressurized fluids may also travel through the permeable beds (e.g., Gay et al. 2006). This is seen in the centre of the study area where an anticline on the late Campanian surface displays a PHAA using the envelope attribute in Fig. 14b. The PHAA anticline is situated directly above the intersection of the compressional and translational domains and is bound within a horst structure (Figs. 13 and 14). Hydrocarbons are therefore both structurally (anticline and horst structure) and stratigraphically (late Campanian surface) trapped. As sedimentation progressed, hydrocarbons migrated upwards through the stratigraphy to the seafloor when later faults formed. Irregular pockmarks on the seafloor, directly above the PHAA anticline, may be explained by this continued seep of hydrocarbons disrupting their normal elliptical/cone-shaped depressions (Figs. 10 and 14).

### Mass wasting features

Slides are observed in the S and centre of the study area, and a major slump scar is observed in the NW on the present-day seafloor (Fig. 10). Slides are known to be coherent masses with minor internal deformation as shown in this study (Fig. 9d), while slumps (a mass flow that is a magnitude higher in flow velocity) are characterised by more internal deformation as seen from the seafloor sediments in Figs. 11b and 12 (Posamentier and Martinsen 2011). These mass wasting features are closely related to gas/fluid escape features found on the seafloor; an elongated mud volcano is found in the centre of the slump scar in the NW (Figs. 10, 11 and 12) and pockmarks are found together with slides in the S (Figs. 9b, d and 10). Both mass wasting features occur

in the distal down-dip region where the slope dips steepest. Possible triggers for mass wasting on the seafloor and the underlying Upper Cretaceous DWFTB system (a different type of mass transport) include seismicity, rapid sedimentation rates upon a dipping slope, high internal pore fluid pressures and downslope undercutting (Séranne and Anka 2005; Rogers and Rau 2006; Kuhlmann et al. 2010). Another trigger mechanism for mass wasting in the Cenozoic is the interaction of opposite-flowing ocean currents along the SW African margin (Weigelt and Uenzelmann-Neben 2004).

High methane expulsion rates associated with sedimentary volcanism (Roberts et al. 2006) destabilized sediments surrounding the elongated mud volcano. This led to major slumping on the seafloor. The size of the slump scar is an indication of how much sediment was (and possibly still is) being remobilized in the underlying stratigraphy—greater than  $26 \times 19$  km. Pockmarks formed under moderate hydrocarbon expulsion rates (Roberts et al. 2006) and consequently, instead of one large slump feature, they are associated with smaller slides which reflect lower flow velocities (Fig. 10). Slope instability leading to these mass wasting features along a dipping slope arise from discontinuities in the subsurface. These discontinuities are faults between the Oligocene to seafloor surfaces leading to pockmark formation and are the gliding planes of some slumps (Figs. 9c and d). Large and irregular seafloor pockmarks in association with slides (Fig. 10) reflect the progressive downslope flow of sediment in mass wasting, i.e., pockmarks grow in size as slides continue downslope along a gliding plane as seen in Fig. 9d. On the seafloor this implies that Cenozoic faults first led to pockmark formation, and some of these very same faults became gliding planes for mass sediment flows (slides). Cenozoic mass wasting features are also observed in the shallower regions of the Orange Basin caused by margin instability and gravity faulting as old, underlying faults were rejuvenated in the outer margin (e.g., Hirsch et al. 2010; Palan et al. 2020).

## Conclusions

The 3D seismic data helped to view natural gas and fluid escape features which would previously have been missed or not fully resolved in a regular 2D survey. This study describes the occurrence of widespread natural gas/fluid escape features in relation to an underlying Upper Cretaceous DWFTB system in the deep-water Orange Basin. Together with the shallow water hydrocarbon systems in play, and encouraging deep-water discoveries in Namibia, the numerous gas/fluid escape features observed in this study point to a prolific hydrocarbon system in the deep-water

South African basin that is yet to be exploited. The following conclusions can be drawn with regards to the origin, distribution and occurrence of gas/fluid escape features, and its implications on the deep-water basin's hydrocarbon system:

- Hydrocarbons are biogenic and mostly thermogenic and in origin, sourced from nutrient-rich Cenozoic sediments and the speculated Turonian source rock, respectively, in addition to the thermogenic Aptian source shales.
- Methane expulsion rates increase from the SE to NW having culminated in an elongated mud volcano situated within an anticline axis of a Upper Cretaceous thrust belt marking the intersection of the translational and compressional domains. The tectonically controlled mud volcano is indicative of extreme overpressures, and thus, rapid rates of methane flux.
- On the seafloor, sediment instability resulted in major slumping in the NW due to sediment remobilization associated with mud volcanism, and smaller slides in the S associated with pockmarks.
- Hydrocarbons migrated in a NW direction following the underlying trend of a Upper Cretaceous thrust belt located at the intersection of the translational and compressional domains.
- The largest accumulation of hydrocarbons, and hence most favourable place to drill is in the region directly above the late Campanian anticline based on it appearing as a PHAA, and the presence of seafloor pockmarks directly above the area.

We recommend drilling to ground truth the observations made to get the exact stratigraphy, ages, depths, rates of gas expulsion and nature of the sediments. This will ultimately determine the economic viability of the deep-water Orange Basin's hydrocarbon system.

**Supplementary Information** The online version contains supplementary material available at <https://doi.org/10.1007/s11001-023-09523-2>.

**Acknowledgements** For funding the first author's doctoral, our sincerest thanks are extended to the National Research Foundation (NRF) of South Africa and the South African Council for Geoscience (CGS), respectively. We would also like to thank Shell and the Petroleum Agency of South Africa (PASA) for providing the 3D reflection seismic data, and Schlumberger for the Petrel software and support. We are furthermore grateful for the scientific discussions and insights provided by our friends and colleagues from the Wits Seismic Research Centre. The authors thank two anonymous reviewers whose comments have greatly improved the manuscript. The authors also thank Dr. Wu-Cheng Chi for editorial handling.

**Author contributions** All authors contributed to the conception and design of the manuscript. NGM conducted the research and wrote the manuscript draft; MSDM and ZJ supervised the main author's research; MSDM, ZJ, and JEB reviewed and edited the manuscript. All authors read and approved the final manuscript.



**Funding** Open access funding provided by University of the Witwatersrand. This study was funded by the National Research Foundation (NRF) of South Africa for the first author's doctoral under grant UID: 130186, and the South African Council for Geoscience (CGS) for the first author's master's degree.

**Data availability** The data are the property of Shell and may be purchased through the Petroleum Agency of South Africa's (PASA) online geoportal at [https://geoportal.petroleumagencysa.com/Storefront/Viewer/index\\_map.html](https://geoportal.petroleumagencysa.com/Storefront/Viewer/index_map.html) (last access: 9 November 2022).

## Declarations

**Competing interests** The authors have no competing interests to declare that are relevant to the content of this manuscript.

**Ethical approval** Not applicable.

**Consent to participate** Not applicable.

**Consent for publication** All authors give consent for publication.

**Open Access** This article is licensed under a Creative Commons Attribution 4.0 International License, which permits use, sharing, adaptation, distribution and reproduction in any medium or format, as long as you give appropriate credit to the original author(s) and the source, provide a link to the Creative Commons licence, and indicate if changes were made. The images or other third party material in this article are included in the article's Creative Commons licence, unless indicated otherwise in a credit line to the material. If material is not included in the article's Creative Commons licence and your intended use is not permitted by statutory regulation or exceeds the permitted use, you will need to obtain permission directly from the copyright holder. To view a copy of this licence, visit <http://creativecommons.org/licenses/by/4.0/>.

## References

- Aizawa M, Bluck B, Cartwright J, Milner S, Swart R, Ward J (2000) Constraints on the geomorphological evolution of Namibia from the offshore stratigraphic record. *Commun Geol Surv Namibia* 12:337–346
- Aldrich, J, Zilinski, R, Edman, J, Leu, W, Berge, T and Corbett, K (2003) Documentation of a new petroleum system in the South Atlantic. In AAPG Annual Convention Salt Lake City, p. 90013
- Andresen KJ (2012) Fluid flow features in hydrocarbon plumbing systems: What do they tell us about the basin evolution? *Mar Geol* 332:89–108. <https://doi.org/10.1016/j.margeo.2012.07.006>
- Andresen KJ, Huuse M (2011) 'Bulls-eye' pockmarks and polygonal faulting in the Lower Congo Basin: relative timing and implications for fluid expulsion during shallow burial. *Mar Geol* 279:111–127. <https://doi.org/10.1016/j.margeo.2010.10.016>
- Anka Z, Loegering M, di Primio R, Marchal D, Rodriguez J, Vallejo E (2014) Distribution and origin of natural gas leakage in the Colorado Basin, offshore Argentina Margin, South America: seismic interpretation and 3D basin modelling. *Geol Acta* 12:269–285. <https://doi.org/10.1344/GeologicaActa2014.12.4.1>
- Baby G, Guillocheau F, Morin J, Ressouche J, Robin C, Broucke O, Dall'Asta M (2018) Post-rift stratigraphic evolution of the Atlantic margin of Namibia and South Africa: implications for the vertical movements of the margin and the uplift history of the South African Plateau. *Mar Petrol Geol* 97:169–191. <https://doi.org/10.1016/j.marpetgeo.2018.06.030>
- Baby G, Guillocheau F, Braun J, Robin C, Dall'Asta M (2020) Solid sedimentation rates history of the Southern African continental margins: implications for the uplift history of the South African Plateau. *Terra Nova* 32:53–65. <https://doi.org/10.1111/ter.12435>
- Ben-Avraham Z, Smith G, Reshef M, Jungslager E (2002) Gas hydrate and mud volcanoes on the southwest African continental margin off South Africa. *Geology* 30:927–930. [https://doi.org/10.1130/0091-7613\(2002\)030%3c0927:GHAMVO%3e2.0.CO;2](https://doi.org/10.1130/0091-7613(2002)030%3c0927:GHAMVO%3e2.0.CO;2)
- Bilotti F, Shaw JH (2005) Deep-water Niger Delta fold and thrust belt modeled as a critical-taper wedge: the influence of elevated basal fluid pressure on structural styles. *AAPG Bull* 89:1475–1491. <https://doi.org/10.1306/06130505002>
- Bolli HM, Ryan WBF, Foresman JB, Hottman WE, Kagami H, Longoria JF, McKnight BK, Melguen M, Natland J, Proto-Decima F (1978) Cape basin continental rise sites 360 and 361. *Init Rep Deep Sea Drill Proj* 40:29–182
- Boyd D, Anka Z, di Primio R, Kuhlmann G, De Wit MJ (2011) Passive margin evolution and controls on natural gas leakage in the Orange Basin, South Africa. *South Afr J Geol* 114:415–432. <https://doi.org/10.2113/gssaj.114.3-4.415>
- Brown KM (1990) The nature and hydrogeological significance of mud diapirs and diatremes for accretionary systems. *J Geophys Res* 95:8969–8982. <https://doi.org/10.1029/JB095iB06p08969>
- Brown R, Summerfield M, Gleadow A, Gallagher K, Carter A, Beucher R, Wildman M (2014) Intracontinental deformation in southern Africa during the late cretaceous. *J Afr Earth Sci* 100:20–41
- Brown LF, Benson JM, Brink GJ, Doherty S, Jollands A, Jungslager EAH, Keenan JHG, Muntingh A, van Wyk NJS (1995) Sequence stratigraphy in offshore south african divergent basins: an atlas on exploration for cretaceous lowstand traps by soekor. *AAPG Studies in Geology*, Tulsa, p 191
- Burnett MD, Castagna JP, Méndez-Hernández E, Rodríguez GZ, García LF, Vázquez JTM, Avilés MT, Villaseñor RV (2003) Application of spectral decomposition to gas basins in Mexico. *Lead Edge* 22:1130–1134. <https://doi.org/10.1190/1.1634918>
- Cartwright JA (1994) Episodic basin-wide fluid expulsion from geopressured shale sequences in the North Sea basin. *Geology* 22:447–450. [https://doi.org/10.1130/0091-7613\(1994\)022%3c0447:EBWFEF%3e2.3.CO;2](https://doi.org/10.1130/0091-7613(1994)022%3c0447:EBWFEF%3e2.3.CO;2)
- Cartwright J (2007) The impact of 3D seismic data on the understanding of compaction, fluid flow and diagenesis in sedimentary basins. *J Geol Soc Lond* 164:881–893. <https://doi.org/10.1144/0016-76492006-14>
- Cartwright J (2011) Diagenetically induced shear failure of fine-grained sediments and the development of polygonal fault systems. *Mar Petrol Geol* 28:1593–1610. <https://doi.org/10.1016/j.marpetgeo.2011.06.004>
- Cartwright J, Santamarina C (2015) Seismic characteristics of fluid escape pipes in sedimentary basins: implications for pipe genesis. *Mar Petrol Geol* 65:126–140. <https://doi.org/10.1016/j.marpetgeo.2015.03.023>
- Cartwright J, Huuse M, Aplin A (2007) Seal bypass systems. *AAPG Bull* 91:1141–1166. <https://doi.org/10.1306/04090705181>
- Cartwright J, James D, Bolton A (2003) The genesis of polygonal fault systems: a review. *Subsurface sediment mobilization. Geol Soc Lond Spec Publ* 216:223–243. <https://doi.org/10.1144/GSL.SP.2003.216.01.15>
- Cathles LM, Su Z, Chen D (2010) The physics of gas chimney and pockmark formation, with implications for assessment of sea-floor hazards and gas sequestration. *Mar Petrol Geol* 27:82–91. <https://doi.org/10.1016/j.marpetgeo.2009.09.010>
- Catuneanu O (2006) Principles of sequence stratigraphy. Elsevier, Amsterdam, p 375
- Chopra S, Marfurt KJ (2005) Seismic attributes — A historical perspective. *Geophysics* 70:3SO–28SO. <https://doi.org/10.1190/1.2098670>

- Clemson J, Cartwright J, Booth J (1997) Structural segmentation and the influence of basement structure on the Namibian passive margin. *J Geol Soc* 154:477–482. <https://doi.org/10.1144/gsjgs.154.3.0477>
- Collier JS, McDermott C, Warner G, Gyori N, Schnabel M, McDermott K, Horn BW (2017) New constraints on the age and style of continental breakup in the South Atlantic from magnetic anomaly data. *Earth Planet Sc Lett* 477:27–40. <https://doi.org/10.1016/j.epsl.2017.08.007>
- Corredor F, Shaw JH, Bilotti F (2005) Structural styles in the deep-water fold and thrust belts of the Niger Delta. *AAPG Bull* 89:753–780. <https://doi.org/10.1306/02170504074>
- Dalton TJS, Paton DA, Needham T, Hodgson N (2015) Temporal and spatial evolution of deepwater fold thrust belts: Implications for quantifying strain imbalance. *Interpretation* 3:SAA59–SAA70. <https://doi.org/10.1190/INT-2015-0034.1>
- Dalton TJS, Paton DA, Needham DT (2017) Influence of mechanical stratigraphy on multi-layer gravity collapse structures: insights from the Orange Basin, South Africa. *Geol Soc Lond Sp Publ* 438:211–228. <https://doi.org/10.1144/SP4384>
- de Vera J, Granado P, McClay K (2010) Structural evolution of the Orange Basin gravity-driven system, offshore Namibia. *Mar Petrol Geol* 27:223–237. <https://doi.org/10.1016/j.marpetgeo.2009.02.003>
- Diester-Haass L, Meyers PA, Bickert T (2004) Carbonate crash and biogenic bloom in the late Miocene: evidence from ODP Sites 1085, 1086, and 1087 in the Cape Basin, southeast Atlantic Ocean. *Paleoceanography*. <https://doi.org/10.1029/2003PA000933>
- Dimitrov LI (2002) Mud volcanoes—the most important pathway for degassing deeply buried sediments. *Earth Sci Rev* 59:49–76. [https://doi.org/10.1016/S0012-8252\(02\)00069-7](https://doi.org/10.1016/S0012-8252(02)00069-7)
- Emery KO, Uchupi E, Bowin CO, Phillips J, Simpson ESW (1975) Continental margin off Western Africa: Cape St Francis (South Africa) to Walvis Ridge (South-West Africa). *AAPG Bull* 59:3–59. <https://doi.org/10.1306/83D91C09-16C7-11D7-8645000102C1865D>
- Feder J (2019) Offshore: making a comeback after the downturn. *J Pet Technol* 71:27–31. <https://doi.org/10.2118/0519-0027-JPT>
- Frimmel HE, Basei MS, Gaucher C (2011) Neoproterozoic geodynamic evolution of SW-Gondwana: a southern African perspective. *Int j Earth Sci Geol* 100:323–354. <https://doi.org/10.1007/s00531-010-0571-9>
- Gay A, Lopez M, Cochonot P, Sultan N, Cauquil E, Brigaud F (2003) Sinuous pockmark belt as indicator of a shallow buried turbiditic channel on the lower slope of the Congo Basin, West African Margin. *Geol Soc Lond Spec Publ* 216:173–189. <https://doi.org/10.1144/GSL.SP.2003.216.01.12>
- Gay A, Lopez M, Cochonot P, Séranne M, Levaché D, Sermondadaz G (2006) Isolated seafloor pockmarks linked to BSRs, fluid chimneys, polygonal faults and stacked Oligocene-Miocene turbiditic palaeochannels in the Lower Congo Basin. *Mar Geol* 226:25–40. <https://doi.org/10.1016/j.margeo.2005.09.018>
- Gay A, Lopez M, Berndt C, Seranne M (2007) Geological controls on focused fluid flow associated with seafloor seeps in the Lower Congo Basin. *Mar Geol* 244:68–92. <https://doi.org/10.1016/j.margeo.2007.06.003>
- Granado P, Vera JD, McClay KR (2009) Tectonostratigraphic evolution of the Orange Basin, SW Africa. *Trabajos de geología* 29:321–328
- Hartwig A, Anka Z, di Primio R (2012) Evidence of a widespread paleo-pockmarked field in the Orange Basin: an indication of an early Eocene massive fluid escape event offshore South Africa. *Mar Geol* 332–334:222–234. <https://doi.org/10.1016/j.margeo.2012.07.012>
- Heins WA (2022) Probing the frontier in Namibia. *First Break* 40:51–57. <https://doi.org/10.3997/1365-2397.fb2022037>
- Henriet JP, De Batist M, Verschuren J (1991) Early fracturing of Palaeogene clays, southernmost North Sea: relevance to mechanisms of primary hydrocarbon migration. *Spec Pub Eur Assoc Petrol* 1:217–227
- Herron DA (2011) Resolution. In: Latimer RB (ed) *First steps in seismic interpretation*. Soc Expl Geophys, Tulsa, pp 75–82
- Hirsch KK, Scheck-Wenderoth M, van Wees J-D, Kuhlmann G, Paton DA (2010) Tectonic subsidence history and thermal evolution of the Orange Basin. *Mar Petrol Geol* 2:565–584. <https://doi.org/10.1016/j.marpetgeo.2009.06.009>
- Ho S, Cartwright JA, Imbert P (2012) Vertical evolution of fluid venting structures in relation to gas flux, in the Neogene-Quaternary of the Lower Congo Basin, Offshore Angola. *Mar Geol* 332:40–55. <https://doi.org/10.1016/j.margeo.2012.08.011>
- Holtar E, Forsberg AW (2000) Postrift development of the Walvis Basin, Namibia: results for the exploration campaign in quadrant 1911. In: Mello MR, Katz BJ (eds) *Petroleum Systems of South Atlantic Margins*. AAPG Mem, Tulsa, pp 429–446
- Hovland M, Judd AG (1988) Seabed pockmarks and seepages: impact on geology, biology and the marine environment. Graham and Trotman Ltd, London, p 293
- Hustoft S, Bünz S, Mienert J (2010) Three-dimensional seismic analysis of the morphology and spatial distribution of chimneys beneath the Nyegga pockmark field, offshore mid-Norway. *Basin Res* 22:465–480. <https://doi.org/10.1111/j.1365-2117.2010.00486.x>
- Huuse M, Jackson CAL, Van Rensbergen P, Davies RJ, Flemings PB, Dixon RJ (2010) Subsurface sediment remobilization and fluid flow in sedimentary basins: an overview. *Basin Res* 22:342–360. <https://doi.org/10.1111/j.1365-2117.2010.00488.x>
- Isiaka AI, Durrheim RJ, Manzi MS, Andreoli MA (2017) 3D seismic analysis of the AK Fault, Orange Basin, South Africa: implications for hydrocarbon leakage and offshore neotectonics. *Tectonophysics* 721:477–490. <https://doi.org/10.1016/j.tecto.2017.10.011>
- Judd AG, Hovland M (2007) *Seabed fluid flow: impact on geology*. Cambridge University Press, Cambridge, *Biology and the Marine Environment*, p 475p
- Judd AG, Long D, Sankey M (1994) Pockmark formation and activity, UK block 15/25, North Sea. *B Geol Soc Denmark* 41:34–49
- Jungslager EH (1999) Petroleum habitats of the Atlantic margin of South Africa. *Geol Soc Lond Sp Publ* 153:153–168. <https://doi.org/10.1144/GSL.SP.1999.153.01.10>
- King LH, MacLean B (1970) Pockmarks on the Scotian shelf. *Geol Soc Am Bull* 81:3141–3148. [https://doi.org/10.1130/0016-7606\(1970\)81\[3141:POTSS\]2.0.CO;2](https://doi.org/10.1130/0016-7606(1970)81[3141:POTSS]2.0.CO;2)
- Koopmann H, Schreckenberger B, Franke D, Becker K, Schnabel M (2016) The late rifting phase and continental break-up of the southern South Atlantic: the mode and timing of volcanic rifting and formation of earliest oceanic crust. *Geol Soc Lond Sp Publ* 420:315–340. <https://doi.org/10.1144/SP420.2>
- Koson S, Chenrai P, Choowong M (2014) Seismic attributes and their applications in seismic geomorphology. *Bull Earth Sci Thai* 6:1–9
- Kramer EAJ, Heck L (2014) Orange basin 3D pre-processing and preSDM 2013 shell global solutions international BV. Rijswijk, Netherlands
- Krueger A, Gilbert E (2009) Deepwater fold-thrust belts: not all the beasts are equal. AAPG search and discovery article 30085. [https://www.searchanddiscovery.com/documents/2009/30085\\_krueger/index.htm](https://www.searchanddiscovery.com/documents/2009/30085_krueger/index.htm). Accessed 9 Nov 2022
- Kuhlmann G, Adams S, Campher C, van der Spuy D, di Primio R, Horsfield B (2010) Passive margin evolution and its controls on natural gas leakage in the southern Orange Basin, blocks 3/4, offshore South Africa. *Mar Petrol Geol* 27:973–992. <https://doi.org/10.1016/j.marpetgeo.2010.01.010>



- L'Arvor E, Maya T, Lattes P (2020) Seismic survey challenges offshore South Africa. In Second EAGE marine acquisition workshop 2020. EAGE Publications BV, pp 1–3
- Lebedeva-Ivanova N, Polteau S, Bellwald B, Planke S, Berndt C, Stokke HH (2018) Toward one-meter resolution in 3D seismic. *Lead Edge* 37:818–828. <https://doi.org/10.1190/tle37110818.1>
- Light MPR, Maslanyj MP, Greenwood RJ, Banks NL (1993) Seismic sequence stratigraphy and tectonics offshore Namibia. *Geol Soc Lond Sp Publ* 71:163–191. <https://doi.org/10.1144/GSL.SP.1993.071.01.08>
- Loncke L, Mascle J, Parties FS (2004) Mud volcanoes, gas chimneys, pockmarks and mounds in the Nile deep-sea fan (Eastern Mediterranean): geophysical evidences. *Mar Petrol Geol* 21:669–689. <https://doi.org/10.1016/j.marpetgeo.2004.02.004>
- Løseth H, Gading M, Wensaas L (2009) Hydrocarbon leakage interpreted on seismic data. *Mar Petrol Geol* 26:304–1319. <https://doi.org/10.1016/j.marpetgeo.2008.09.008>
- Løseth H, Wensaas L, Gading M (2011) Deformation structures in organic-rich shales. *AAPG Bull* 95:729–747. <https://doi.org/10.1306/09271010052>
- Maduna NG, Manzi MS, Jinnah Z, Bourdeau JE (2022) Strato-structural evolution of the deep-water Orange Basin: constraints from 3D reflection seismic data. *Solid Earth* 13:1755–1780. <https://doi.org/10.5194/se-13-1755-2022>
- Mahlalela V, Manzi MSD, Jinnah Z, Bourdeau JE, Durrheim RJ (2021) Structural characteristics and 3D seismic detection of gas migration pathways in the deep-water Orange Basin. *S Afr Mar Geophys Res* 42:8. <https://doi.org/10.1007/s11001-021-09428-y>
- Manzi MSD, Durrheim RJ, Hein KAA, King N (2012) 3D edge detection seismic attributes used to map potential conduits for water and methane in deep gold mines in the Witwatersrand basin, South Africa. *Geophysics* 77:W133–W147. <https://doi.org/10.1190/geo2012-0135.1>
- Manzi MSD, Hein KAA, King N, Durrheim RJ (2013) Neoproterozoic tectonic history of the Witwatersrand Basin and Ventersdorp Supergroup: new constraints from high-resolution 3D seismic reflection data. *Tectonophysics* 590:94–105. <https://doi.org/10.1016/j.tecto.2013.01.014>
- Maselli V, Kneller B, Taiwo OL, Iacopini D (2019) Sea floor bedforms and their influence on slope accommodation. *Mar Pet Geol* 102:625–637. <https://doi.org/10.1016/j.marpetgeo.2019.01.021>
- Maslanyj MP, Light MPR, Greenwood RJ, Banks NL (1992) Extension tectonics offshore Namibia and evidence for passive rifting in the South Atlantic. *Mar Petrol Geol* 9:590–601. [https://doi.org/10.1016/0264-8172\(92\)90032-A](https://doi.org/10.1016/0264-8172(92)90032-A)
- Mazzini A, Etiope G (2017) Mud volcanism: an updated review. *Earth Sci Rev* 168:81–112
- Mazzini A, Nermoen A, Krotkiewski M, Podladchikov Y, Planke S, Svensen H (2009) Strike-slip faulting as a trigger mechanism for overpressure release through piercement structures. Implications for the Lusi mud volcano. *Indonesia Mar Pet Geol* 26:1751–1765. <https://doi.org/10.1016/j.marpetgeo.2009.03.001>
- Menzies MA, Klempner SL, Ebinger CJ, Baker J (2002) Characteristics of volcanic rifted margins. In: Menzies MA, Klempner SL, Ebinger CJ, Baker J (eds) *Volcanic rifted margins*. Geological Society of America, Boulder, pp 1–14. <https://doi.org/10.1130/0-8137-2362-0.1>
- Mitchum RM, Vail PR, Thompson S (1977) Seismic stratigraphy and global changes of sea level: Part 2. The depositional sequence as a basic unit for stratigraphic analysis: Section 2. Application of seismic reflection configuration to stratigraphic interpretation. *AAPG Memoir*, Tulsa, pp 53–62
- Mohammed M, Paton D, Collier REL, Hodgson N, Negonga M (2017) Interaction of crustal heterogeneity and lithospheric processes in determining passive margin architecture on the southern Namibian margin. *Geol Soc Lond Sp Publ* 438:177–193. <https://doi.org/10.1144/SP438.9>
- Morley CK, King R, Hillis R, Tingay M, Backe G (2011) Deepwater fold and thrust belt classification, tectonics, structure and hydrocarbon prospectivity: a review. *Earth-Sci Rev* 104:41–91. <https://doi.org/10.1016/j.earscirev.2010.09.010>
- Naseer MT, Asim S (2017) Detection of cretaceous incised-valley shale for resource play, Miano gas field, SW Pakistan: spectral decomposition using continuous wavelet transform. *J Asian Earth Sci* 47:358–377. <https://doi.org/10.1016/j.jseaeas.2017.07.031>
- Nemčok M, Schamel S, Gayer R (2005) *Thrustbelts: Structural architecture, thermal regimes and petroleum systems*, 1st edn. Cambridge University Press, Cambridge, pp 1–541
- Palan K, Green AN, Andrews B, Sink K, Wiles EA (2020) A morphometric analysis of the fluid flow features of the southern Orange Basin South Africa. *Mar Geol*. <https://doi.org/10.1016/j.margeo.2020.106145>
- Paton DA, di Primio R, Kuhlmann G, van der Spuy D, Horsfield B (2007) Insights into the petroleum system evolution of the southern Orange Basin, South Africa. *South Afr J Geol* 110:261–274. <https://doi.org/10.2113/gssajg.110.2-3.261>
- Paton DA, van der Spuy D, di Primio R, Horsfield B (2008) Tectonically induced adjustment of passive-margin accommodation space; influence on the hydrocarbon potential of the Orange Basin, South Africa. *AAPG Bull* 92:589–609. <https://doi.org/10.1306/12280707023>
- Petroleum Agency South Africa (PASA) (2017) Information and opportunities, Petroleum Agency South Africa, Cape Town, South Africa. [https://www.petroleumagencyrsa.com/images/pdfs/Pet\\_expl\\_opp\\_broch\\_2017bw1.pdf](https://www.petroleumagencyrsa.com/images/pdfs/Pet_expl_opp_broch_2017bw1.pdf). Accessed 9 Nov 2022
- Planke S, Svensen H, Hovland M, Banks DA, Jamtveit B (2003) Mud and fluid migration in active mud volcanoes in Azerbaijan. *Geo-Mar Lett* 23:258–268. <https://doi.org/10.1007/s00367-003-0152-z>
- Posamentier HW, Martinsen OJ, Shipp RC (2011) The character and genesis of submarine mass-transport deposits: insights from outcrop and 3D seismic data. *Mass-transport deposits in deepwater settings*. SEPM Special Publication, Tulsa, pp 7–38
- Randen T, Monsen E, Signer C, Abrahamson A, Hansen JO, Sæter T, Schlaf J (2000) Three-dimensional texture attributes for seismic data analysis. In: 2000 SEG Annual Meeting, pp 668–671. <https://doi.org/10.1190/1.1816155>
- Roberts HH, Hardage BA, Shedd WW, Hunt J Jr (2006) Seafloor reflectivity—An important seismic property for interpreting fluid/gas expulsion geology and the presence of gas hydrate. *Lead Edge* 25:620–628. <https://doi.org/10.1190/1.2202667>
- Rogers J, Rau A (2006) Surficial sediments of the wave-dominated Orange River Delta and the adjacent continental margin off south-western Africa. *Afr J Mar Sci* 28:511–524. <https://doi.org/10.2989/18142320609504202>
- Rommerskirchen F, Condon T, Mollenhauer G, Dupont L, Schefuß E (2011) Miocene to Pliocene development of surface and subsurface temperatures in the Benguela current system. *Paleoceanography* 26:1–15. <https://doi.org/10.1029/2010PA002074>
- Rowan MG, Peel FJ, Vendeville BC (2004) Gravity-driven fold belts on passive margins. In: McClay KR (ed) *Thrust tectonics and hydrocarbon systems*. AAPG Bull, Tulsa, pp 157–182
- Scarselli N, McClay K, Elders C (2016) Seismic geomorphology of cretaceous megaslides offshore Namibia (Orange Basin): Insights into segmentation and degradation of gravity-driven linked systems. *Mar Petrol Geol* 75:151–180. <https://doi.org/10.1016/j.marpetgeo.2016.03.012>
- Schoole L, Manzi MS, Zhang SE, Bourdeau JE (2020) An innovative seismic and statistical approach to understand 3D magmatic structures and ore deposits in the western Bushveld Complex. S

- Afr. Ore Geol Rev 126:103784. <https://doi.org/10.1016/j.oregeorev.2020.103784>
- Séranne M, Anka Z (2005) South Atlantic continental margins of Africa: a comparison of the tectonic vs climate interplay on the evolution of equatorial west Africa and SW Africa margins. *J Afr Earth Sci* 43:283–300. <https://doi.org/10.1016/j.jafrearsci.2005.07.010>
- Silva CC, Marcolino CS, and Lima FD (2005) Automatic fault extraction using ant tracking algorithm in the Marlim South Field, Campos Basin. Paper presented at the 2005 SEG Annual Meeting, Houston, Texas, 6–11 November 2005, 857–860. <https://doi.org/10.1190/1.2148294>
- van der Spuy D, Sayidini B (2022) Offshore Namibia discovery signals bright future for South Africa oil and gas. *AAPG Explorer*. <https://explorer.aapg.org/story/articleid/62613/offshore-namibia-discovery-signals-bright-future-for-south-africa-oil-and-gas>. Accessed 31 Mar 2022
- Uenzelmann-Neben G, Tobias W, Gruetzner J, Maik T (2017) Transition from the Cretaceous ocean to Cenozoic circulation in the western South Atlantic—a twofold reconstruction. *Tectonophysics* 716:22–240. <https://doi.org/10.1016/j.tecto.2016.05.036>
- van der Spuy D (2003) Aptian source rocks in some South African Cretaceous basins. *Geol Soc Lond Sp Publ* 207:185–202. <https://doi.org/10.1144/GSL.SP.2003.207.10>
- Viola G, Andreoli M, Ben-Avraham Z, Stengel I, Reshef M (2005) Offshore mud volcanoes and onland faulting in southwestern Africa: neotectonic implications and constraints on the regional stress field. *Earth Planet Sci Lett* 231:147–160. <https://doi.org/10.1016/j.epsl.2004.12.001>
- Viola G, Kounov A, Andreoli MAG, Mattila J (2012) Brittle tectonic evolution along the western margin of South Africa: more than 500 Myr of continued reactivation. *Tectonophysics* 514:93–114. <https://doi.org/10.1016/j.tecto.2011.10.009>
- Weigelt E, Uenzelmann-Neben G (2004) Sediment deposits in the Cape Basin: indications for shifting ocean currents? *AAPG Bull* 88:765–780. <https://doi.org/10.1306/01260403101>
- Wildman M, Brown R, Watkins R, Carter A, Gleadow A, Summerfield M (2015) Post break-up tectonic inversion across the southwestern cape of South Africa: New insights from apatite and zircon fission track thermochronometry. *Tectonophysics* 654:30–55. <https://doi.org/10.1016/j.tecto.2015.04.012>
- Yilmaz Ö (2001) *Seismic data analysis: Processing, inversion, and interpretation of seismic data*. Society of Exploration Geophysicists, Tulsa

**Publisher's Note** Springer Nature remains neutral with regard to jurisdictional claims in published maps and institutional affiliations.